Summer 8-15-2018

Controlling the Oxygen Microenvironment: The Role of HIF-1α in Early Tumor Progression

Sandra Lam
Washington University in St. Louis

WASHINGTON UNIVERSITY IN ST. LOUIS

School of Engineering & Applied Science
Department of Biomedical Engineering

Dissertation Examination Committee:
Steven George, Chair
Lori Setton, Co-Chair
Samuel Achilefu
Gregory Longmore
Larry Taber

Controlling the Oxygen Microenvironment: The Role of HIF-1α in Early Tumor Progression

by
Sandra Lam

A dissertation presented to
The Graduate School
of Washington University in
partial fulfillment of the
requirements for the degree
of Doctor of Philosophy

August 2018
St. Louis, Missouri

Table of Contents

List of Figures iv
List of Tables v
Acknowledgments vi
Abstract of the Dissertation viii
Chapter 1: Background and Motivation 1
2.1 Overview 4
2.2 Controlling and Measuring Oxygen *in vitro* 5
Chapter 3: Microfluidic device to attain high spatial and temporal control of oxygen 8
3.1 Abstract 8
3.2 Introduction 9
3.3 Materials and Methods 11
3.3.1 Design and microfabrication of microfluidic device 11
3.3.2 Numerical Simulations 13
3.3.3 Oxygen Measurements 15
3.3.4 Cell Culture 16
3.3.5 Device Experimentation 17
3.3.6 Quantification of Biased Angiogenesis 18
3.3.7 Statistical Analysis 19
3.4 Results 19
3.4.1 Microfluidic Device: Pressure and Flow 19
3.4.2 Microfluidic Device: Oxygen Concentration Profiles 20
3.4.3 Angiogenesis within the three-chambered device 24
3.5 Discussion 26
3.6 Conclusion 28
Chapter 4: Knockdown of HIF-1α Affects MDA-MB-231 Survival under Spatial and Temporal Oxygen Gradients 29
4.1 Abstract 29
4.2 Introduction 30
4.3 Methods 31

4.3.1 Construction of Microfluidic Device 31
4.3.2 Finite Element Modeling 33
4.3.3 MDA-MB-231 Cell Culture 33
4.3.4 HIF-1α Knockdown in MDA-MB-231 34
4.3.5 Microfluidic Device Experiment 34
4.3.6 Tumor Growth and Migration Quantification 36
4.3.7 Statistical Analysis 36
4.4 Results 37
4.4.1 Microfluidic Device and Oxygen Concentration Profiles 37
4.4.2 Response of MDA-MB-231 to Varying Oxygen Gradients 38
4.4.3 Scramble and shHIF-1α Growth under Varying Oxygen Gradients 40
4.4.4 Migration parameter during hypoxic conditions 44
4.5 Discussion 45
4.6 Conclusions 47
Chapter 5: Conclusions and Future Directions 49
5.1 Tumor-on-a-chip Systems 49
5.3 Future Directions 52
References 53

List of Figures

Fig. 2. 1 7

Fig. 3. 1 Microfluidic Device Schematic…….....12

Fig. 3. 2 Microfluidic Device Characterization 20

Fig. 3. 3 Finite Element Simulations and Measurements of Steady State Oxygen Tension 21

Fig. 3. 4 Varying Device Parameters 24

Fig. 3. 5 Biased Angiogenesis Due to Hypoxia. 26

Fig. 4. 1 Device Schematic……32

Fig. 4. 2 Model of the oxygen distributions for various sodium sulfite concentrations 37

Fig. 4. 3 There is enhanced tumor progression at 5% O_2 compared to 20% 0_2 for Control MDA-MB-231 cells..... 38

Fig. 4. 4 Varying spatial and temporal gradients do not affect Control cell survival 39

Fig. 4. 5 Relative Gene Expression of Scramble and shRNA HIF-1α cells 40

Fig. 4. 6 Knockdown of HIF-1α impacts tumor progression at normoxia..... 41

Fig. 4. 7 Various oxygen concentration gradients modulate the survival of MDA-MB-231 cells with a knockdown of HIF-1α..... 42

Fig. 4. 8 Percent tumor growth of shHIF-1α..... 43

Fig. 4. 9 Temporal variations in oxygen tension affect the survival of shHIF-1α cells 44

Fig. 4. 10 Knockdown of HIF-1α impacts the migration of MDA-MB-231 cells..... 45

List of Tables

Table 3. 1 List of Model Parameters. 14

Table 3. 2 List of Experimental Conditions 15

Acknowledgments

First, I would like to thank my advisor and committee chair, Professor Steven C. George, for his mentorship through my graduate studies. His enthusiasm and commitment for "doing better science" has been extremely encouraging and helpful over the past couple of years.

I would also like to express sincere gratitude to the members of the George lab, whose involvement made this dissertation possible. Specifically, Dr. Yosuke Kurokawa, Dr. Luis Alonzo, Dr. David Tran, Dr. Monica Moya, Dr. Venktesh Shirure, Dr. Drew Glaser, Dr. Priscilla Hwang, Dr. Mary Kathyrn Sewell-Loftin, Dr. Kuo-Chan Weng, Dr. Bhupinder Shergill, Kyaw Thu Minn, Matt Curtis, Cristi King, Yunli Emily Chu, and Natalie Ng.

Special thanks to Springer International Publishing AG for their permission to include Chapter Two of dissertation, which was originally published in Tumor Organoids.

Financial support was provided by National Heart, Lung, and Blood Institute (NHLBI) T32 fellowship (NIH RC1ES018361) and the National Science Foundation Graduate Research Fellowship (DGE-1143954).

Finally, I would like to express my deepest appreciation for the support from my family and friends whose encouragement motivated me through this process.

Sandra Lam

Washington University in St. Louis

August 2018

Dedicated to my family for their unwavering support.

ABSTRACT OF THE DISSERTATION

Controlling the Oxygen Microenvironment: The Role of HIF-1α in Early Tumor Progression

by

Sandra Lam

Doctor of Philosophy in Biomedical Engineering

Washington University in St. Louis, 2018

Professor Steven George, Chair

Professor Lori Setton, Co-Chair

Cancer drug efficacy has remained a critical obstacle for researchers as it has one of the lowest probabilities of success compared to other diseases. One method to help improve this success rate is to create better tumor models on which to perform the drug testing. With growing interesting in microphysiological systems, scientists can create more advanced *in vitro* models of human organ systems as well as diseased states. These "organ-on-a-chip" platforms aim to improve drug response prediction for both efficacy and toxicity. One underappreciated characteristic of many disease states is that they are often at a lower oxygen tension that normal tissue (a condition known as hypoxia). Not only is this the case for cancer, but it is thought to be one of the main reasons why cancer treatment fails. Furthermore, cancer can experience two types of hypoxia: chronic (sustained low oxygen tension) or intermittent (varying cycles of hypoxia and normoxia). In both conditions, the vasculature determines the spatial and temporal dynamics of oxygen. If the tumor cells expand far enough away from the vasculature, this diffusion-limited oxygen condition will lead to chronic hypoxia. On the other hand, if the tumor cells encourage rapid vasculature growth that tends to be tortuous and leaky, then this will lead to intermittent hypoxia. Under both hypoxic conditions, tumor cells upregulate hypoxia inducible

factor 1α (HIF-1α), a transcription factor which affects many downstream processes that encourages cell survival. In this dissertation, we investigate our ability to use a microfluidic platform to mimic some of these key features in the hypoxic tumor microenvironment and test if it can recapitulate some known biological responses.

First, we created a microfluidic device that can control both spatial and temporal gradients of oxygen via an oxygen scavenger line. As tumor angiogenesis is a major concern during tumor progression, we examined angiogenesis in the device. Vasculature was grown in the central chamber of the device, and stromal cells were grown in compartments on both sides of the vasculature. Lastly, the oxygen scavenger was flown in a channel adjacent to the left stromal chamber to create an oxygen gradient across the device. By controlling the flow the of oxygen scavenger, we could simulate both chronic and intermittent hypoxia. Our results demonstrate that stromal cells under hypoxia conditions encourage biased angiogenesis, which is in agreement with previous studies.

Second, using our microfluidic device platform, we investigated how knocking down HIF-1α affects the survival and progression of breast cancer cells (MDA-MB-231) under various oxygen gradients. By varying the scavenger concentration, we found a threshold for chronic hypoxia that the knockdown cells could no longer survive. Interestingly, by modulating the length of the hypoxic and normoxic cycles during intermittent hypoxia, we could dictate tumor cell survival. This result emphasizes the importance of understanding the temporal variations of oxygen, especially with cancer treatments that target HIF-1α.

Altogether, our results further our understanding of how to control spatial and temporal oxygen gradients for disease modeling. Hopefully with this understanding, future studies will be able to more effectively assess drug efficacy.

Chapter 1: Background and Motivation

Cancer is the second leading cause of death in the United States of America behind heart disease.[1] While the number of deaths from heart disease has decreased ever since 1985, the number of deaths from cancers has nearly tripled since 1960.[2] In addition, it has been estimated that the National Cancer Institute (NCI) alone receives more than $5 billion dollars in government funding yearly.[3] However, there has yet to be a cancer treatment that is effective for all patients. Meanwhile, the cost of developing a pharmaceutical drug is on the rise; the current estimate is $1.3 to $2.6 billion to develop a single drug approved by the US Food and Drug Administration (FDA).[4,5] One solution to curb the rising development costs is to create better models for drug testing.[5]

There are many difficulties associated with mimicking the tumor microenvironment. Perhaps the most important is the shear complexity of the tumor microenvironment; that includes an array of cell types. For example, there is close interaction between the growing tumor and vasculature. While angiogenesis remains quiescent for the most part in adults, in tumor progression, the "angiogenesis switch" remains on constantly.[6] This is because the rapidly growing tumor requires nutrients and oxygen as well as to discard metabolic byproducts and carbon dioxide. Furthermore, access to a vascular network provides tumor cells a method for intravasation and metastasis.[7] These instances are of particular interest to study because the five-yea survival rate of patients with breast cancer metastasis drop dramatically to 22%.[8]

To promote tumor angiogenesis, as the tumor grows, it further depletes oxygen via cellular consumption. This condition of low oxygen (hypoxia) is often associated with poor patient outcome.[9] While a normal tissue response is cellular necrosis, cancer cells have developed an

adaptive mechanism that allows them to thrive in hypoxia.[10] In addition, advanced cancer is typically associated with an oxygen tension that is much lower than normal physiology.[10] Under this condition, cancers tend to resistant to traditional cancer treatments such as chemotherapy and radiotherapy. This effect has largely been attributed to the stabilization of transcriptional regulator, hypoxia-inducible factor 1-alpha (HIF-1α).[11] In cancer biology, this transcription factor is often dysregulated and overexpressed. Thus, one strategy to develop effective cancer treatments in a more efficient manner is to replicate this hypoxia microenvironment during drug testing.[9]

There are several reasons why it is difficult to replicate the oxygen gradients in the tumor microenvironment. First, normal physiology is around 5% O_2, the hypoxic tumor microenvironment can be less than 1% O_2, and atmospheric oxygen is about 20% O_2.[12] This means that cell cultures grown at atmospheric oxygen are experiencing hyperoxia. Second, some research groups choose to set their incubators to a hypoxic oxygen tension, such as 1% O_2. However, this approach does not have the ability to create and control spatial oxygen gradients that are present in normal physiology.[13] Lastly, another strategy to studying hypoxia is to use a compound such as cobalt chloride that will stabilize HIF-1α during normoxia.[14,15] While this makes working with the cell cultures easier, it limits the study to only those signaling mechanisms that are downstream of HIF-1α. In addition, this method also does not replicate the oxygen gradients are present during tumor progression.

Furthermore, while few studies observe the effects of true hypoxia, most only focus on chronic hypoxia (sustained low oxygen tension) and not intermittent hypoxia (cycles of hypoxia and normoxia). However, it has been hypothesized that intermittent hypoxia is more representative of the tumor microenvironment due to the abnormalities of the vasculature due to rapid

angiogenesis.[16] However, this phenomenon has been severely underappreciated due to the difficulties in not only controlling the spatial distribution of oxygen, but the temporal distribution as well.

One potential solution to recapitulating the oxygen dynamics of the tumor microenvironment is to use microfluidic devices. Typically, this type of device will have a scavenger channel dedicated to introducing an oxygen scavenger near the tumor culture chamber. This creates an oxygen sink that will draw oxygen away from the tissue culture. Additionally, due to their inherently small size, diffusion is rapid allowing specified oxygen gradients to be precisely controlled spatially and temporally. This type of platform allows for growing 3D cell culture as well as the ability to include different cell types. By utilizing these aspects of microfluidic devices, the microenvironment during tumor progression can be closely recapitulated.

The dissertation contains 4 subsequent chapters. Chapter 2 overviews the current trends and technologies of tumor hypoxia systems, with an emphasis on tumor development. Chapter 3 focuses on the development of a microfluidic devices to manipulate oxygen tensions within a 3D tissue to study hypoxia induced angiogenesis. Chapter 4 examines the role of HIF-1α in tumor cells during spatial and temporal variations in hypoxia. Lastly, chapter 5 remarks on future advances that can significantly advance the current state of studying tissue hypoxia.

Chapter 2: Hypoxia and Tumor Angiogenesis

2.1 Overview

The deficiency of oxygen, an essential nutrient for cell proliferation and survival, is a critical stimulus for acquiring new blood vessels. Hypoxic tumors activate molecular programs that lead to secretion of proangiogenic factors by the tumor as well as tumor-associated stromal cells. Tumor hypoxia has been associated with poor patient prognosis, with clinical studies showing that advanced breast cancers have a median oxygen tension of 10 mmHg, compared with 65 mmHg in normal breast tissue.[10,17,18] Hypoxic cores exist in advanced stage tumors,[19] and can also exist in tumors as small as 400 μm in diameter.[20] In hypoxic conditions, angiogenesis is primarily regulated by hypoxia inducible factors (HIFs). Of the highly conserved HIF family of transcription factors, HIF-1 has been the best studied.[11,21,22] It is known to be a heterodimer of α-subunit (HIF-1α) and a β-subunit (HIF-1β), where subunits are members of the basic helix-loop-helix (bHLH)-containing PER-ARNT-SIM (PAS) domain family of transcription factors. In addition to HIF-1α and HIF-1β, there are two additional oxygen regulated α-subunits are (HIF-2α and HIF-3α) and two other constitutively expressed β-subunits (HIF-2β, and HIF-3β). Furthermore, the low oxygen environment stabilizes HIF-1α in endothelial cells as well.[23]

The HIF-1 activation follows a series of molecular events. Starting at oxygen concentrations below 6%, HIF-1α stabilizes and translocates from the cytoplasm to the nucleus, where it dimerizes with HIF-1β.[24] HIF-1 then binds to hypoxia responsive elements (HREs) within the promoters of HIF target genes leading to the increased expression of proangiogenic factors such as vascular endothelial growth factor (VEGF), VEGF-R2, angiopoietin 1/2, fibroblast growth factor, platelet-derived growth factor, and the decreased expression of anti-angiogenic factors

such as thrombospondin-1 and carbonic anhydrase-9.[25] In addition to angiogenesis, HIF-1 can activate more than a hundred genes that control important cellular processes such as epithelial-mesenchymal transition, stem-cell maintenance, and metabolism that impact tumor cell invasion, metastasis, metabolic reprograming, and resistance to therapy.[22]

2.2 Controlling and Measuring Oxygen *in vitro*

The traditional method to create hypoxic conditions utilizes cell culture incubators, where blending excess nitrogen with air lowers oxygen concentration. Alternatively, the exchange of oxygen from air can be controlled by an air tight glove box equipment, or hypoxic conditions can simply be generated due to consumption of oxygen by cell culture. Additionally, chemicals that consume oxygen, such as sodium nitrate, can also be used to manipulate oxygen tension.[12] Alternatively, cobalt chloride can stabilize HIF-1α in the presence of normoxia, and allows for more flexible data collection. This "pseudo-hypoxic" condition can simulate the impact of HIF-1α, but cannot fully recapitulate all features that hypoxia has on cell function.[15]

Microfluidic devices have become attractive systems to study hypoxia due to their inherently small size, and thus small diffusion distances. A common technique to reduce oxygen in microfluidic devices is to use separate channels containing an oxygen scavenger such as sodium nitrate (Fig. 2. 1A). These channels are separated from the tissue chambers by a semipermeable material, such as PDMS, that allows diffusion of oxygen but not water.[26–28] By altering the concentration and flow of the scavenger, the oxygen tension within the device can be controlled with high spatial and temporal resolution. PDMS is ideally suited as a material of construction for these device as it is a highly permeable material with respect to oxygen compared to relatively impermeable materials such as cyclic olefin copolymer, polystyrene, polypropylene, poly(methacrylic acid), polyurethane, and poly(methyl pentene).[29] By choosing an appropriate

coating and/or using an oxygen scavenger, a wide range of oxygen concentrations can be controlled to study tumor hypoxia and its effects.

A major advantage of using *in vitro* systems is that real time oxygen measurements can be performed in a live tissue culture with minimal disruption of biological processes. The gold standard for the oxygen sensors is Clark-type electrodes which measure oxygen by detecting a current flow caused by the reduction of oxygen.[30] However, the method is operationally complex and less sensitive for oxygen measurement relative to other methods. Recently, more sensitive techniques have been developed that employs an oxygen sensitive luminophore. The luminescence of oxygen sensitive dyes is inversely proportional to the concentration of oxygen. When the dyes are excited by a laser in the presence of oxygen, the excited state energy of the phosphorescent indicator molecule is absorbed by oxygen instead of being emitted as a luminescent photon. In other words, oxygen quenches the phosphorescence, and reduces the lifetime of the phosphorescence decay. Generally, a shorter luminescence lifetime indicates a higher oxygen concentration. The lifetime of the phosphorescence, as opposed to the intensity, is a more robust method as it is insensitive to photobleaching and independent of the concentration of the dye. Detecting the luminescence lifetime generally requires a more complicated experimental setup because a pulsed laser needs to be used (Fig. 2. 1B).[31]

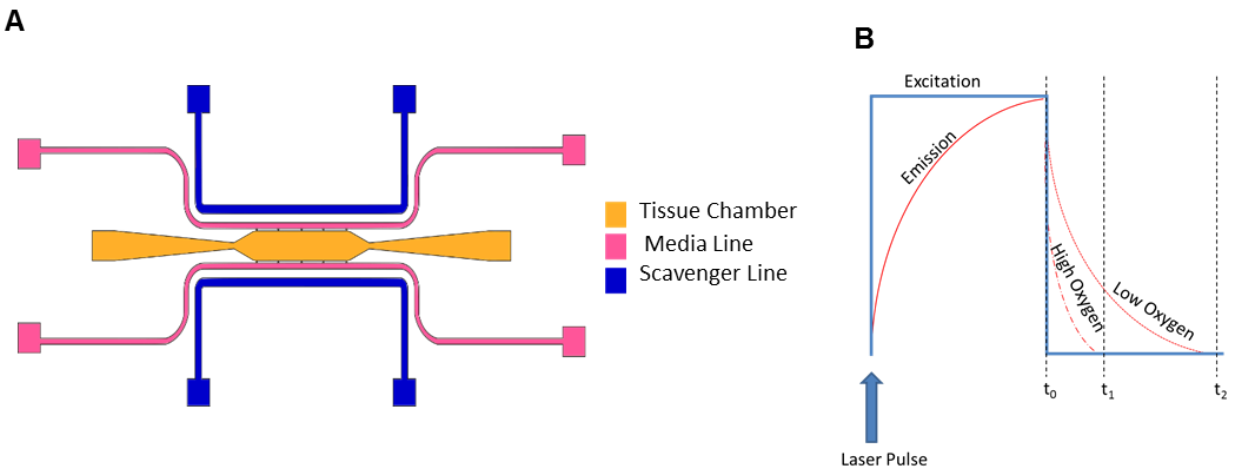

Fig. 2. 1 (A) Oxygen scavenger lines can be designed into microfluidic platforms to generate hypoxic conditions inside tissue chambers. Typically these include materials such as sodium sulfite. (B) PhLM is a method used to measure oxygen concentrations in 3D culture systems. Using a pulsed laser to excite the oxygen sensitive dye and measuring the dye's lifetime of decay, a longer phosphorescent lifetimes correspond to lower oxygen concentrations.

While many research groups have focused on controlling the oxygen environment around tumor spheroids, some groups, including ours, have begun to control oxygen tension in vascularized tumors.[26,27,32] Due to the role that the vascular network has in oxygen regulation and the interaction between the tumor and the vasculature during hypoxia, the inclusion of these components in the next generation of tumor organoid models is critical for a complete understanding of angiogenesis in the tumor microenvironment.

Chapter 3: Microfluidic device to attain high spatial and temporal control of oxygen

3.1 Abstract

Microfluidic devices have been successfully used to recreate *in vitro* biological microenvironments, including disease states. However, one constant issue for replicating microenvironments is that atmospheric oxygen concentration (20% O_2) does not mimic physiological values (often around 5% O_2). We have created a microfluidic device that can control both the spatial and temporal variations in oxygen tensions that are characteristic of *in vivo* biology. Additionally, since the microcirculation is responsive to hypoxia, we used a 3D sprouting angiogenesis assay to confirm the biological relevance of the microfluidic platform. Our device consists of three parallel connected tissue chambers and an oxygen scavenger channel placed adjacent to these tissue chambers. Experimentally measured oxygen maps were constructed using phosphorescent lifetime imaging microscopy and compared with values from a computational model. The central chamber was loaded with endothelial and fibroblast cells to form a 3D vascular network. Four to six days later, fibroblasts were loaded into the side chambers, and a day later the oxygen scavenger (sodium sulfite) was flowed through the adjacent channel to induce a spatial and temporal oxygen gradient. Our results demonstrate that both constant chronic and intermittent hypoxia can bias vessel growth, with constant chronic hypoxia showing higher degrees of biased angiogenesis. Our simple design provides consistent control of spatial and temporal oxygen gradients in the tissue microenvironment and can be used to investigate important oxygen-dependent biological processes in diseases such as cancer and ischemic heart disease.

3.2 Introduction

Although hypoxia, or low oxygen tension, is a central feature of many different diseases, it is also a part of normal physiological states.[10,25,33] Hypoxia can be chronic (sustained oxygen tension < 5% O_2 for > 24 hours), as in the case of ischemic heart disease and wound healing, or intermittent (repeated oxygen tension <5% O_2 for < 24 hours) as in the case of some tumors, sleep apnea, and exercise.[34–37] Moreover, diseases such as cancer can exhibit both chronic hypoxia and intermittent hypoxia states which can affect different processes of tumor progression. The rapid rate of diffusion of abundant oxygen in gas and liquid systems has made it difficult to experimentally study the impact of hypoxia at small spatial scales, in particular, to replicate in vivo intermittent hypoxia conditions. The presence of atmospheric air (ambient pO_2 is around 160 mmHg or 20% O_2) provides a regular source of "contamination" as normoxia or physiological oxygen concentration for tissues are on average about 38 mmHg or 5% O_2. Although previous literature has defined normoxia as 20% O_2, we choose to define it as 5% O_2 because it is more physiologically relevant. Although the incubator oxygen tension may be set to 5% O_2, controlling the spatial distribution of oxygen within the cell culture is not possible. As the tissue expands farther away from the vessel network, an oxygen gradient is established, with the cells farthest away experiencing the lowest oxygen tension. In addition, it has been shown that gradients are important for chemical and mechanical factors for recapitulating the physiological microenvironment.[38,39]

Here, we present a microfluidic device that can precisely control oxygen tension over spatial and temporal dimensions on the order of microns and minutes, respectively. This level of control permits the interrogation of physiologically relevant hypoxia in a wide range of normal and diseased tissues. Our strategy leverages the small dimensions of microfluidic devices that

minimize the distance of diffusion for oxygen to control precise gradients. Microfluidic systems provide faster oxygen cycle switching than some commercial systems, (e.g., Eppendorf Galazy 48R), which can take up to 30 minutes to equilibrate to a new oxygen concentration. In addition, previous methods of studying hypoxia in microfluidic devices often involve nearby channels to flow nitrogen gas to create an oxygen sink.[26,40,41] While this can create controlled oxygen gradients, the need for nitrogen tanks is cumbersome. Furthermore, the use of a compressed gas can introduce bubbles and pervaporation in the culture chambers, which can compromise the experimental conditions.

Our approach utilizes a simple and inexpensive aqueous solution of sodium sulfite as an oxygen scavenger to reduce pervaporation and cost while still maintaining high spatial and temporal control of oxygen. This easily prepared solution is flowed in a fluidic channel running parallel to the tissue chambers. Because this channel is not connected to the tissue chambers the oxygen scavenger will not produce any unwanted side effects to the tissues. Moreover, most in vitro studies mimic intermittent hypoxia cycle between 20% and 1% O_2 to ensure two different oxygen states.[42–44] However, 20% O_2 is representative of hyperoxia and does not accurately represent in vivo intermittent hypoxia. Subsequently, because we can measure the spatial and temporal oxygen distribution within our device, we can easily switch between the more physiological concentration of 5% and 1% O_2. Thus, we believe that our results more accurately represent physiological response to intermittent hypoxia. Furthermore, although previous studies have shown the effects of using an oxygen scavenger in a 20% O_2 incubator the range of oxygen concentrations often go far above physiological values.[45]

To demonstrate the biological relevance of our microfluidic system, we used an in vitro model of angiogenesis. During hypoxia, new blood vessels can sprout from existing vessels (angiogenesis)

as a normal biological response to relieve hypoxia by increasing blood flow and delivering oxygen. On the other hand, hypoxia can also lead to necrosis of the tissue if there is a failure to encourage new vessel growth. These two drastically different outcomes are both possible during hypoxia because both pro-angiogenic and anti-angiogenic genes can be activated, and this balance dictates the outcome.[46] Thus, it is important to determine the subtleties of spatial and temporal variations in oxygen and how this can bias vessel growth. Our theoretical and experimental results demonstrate spatial and temporal control over the oxygen tension within a microfluidic platform. In addition, the simple and flexible design will prove useful for a range of additional biological applications. In this study we show the effects of normoxia (N), constant chronic hypoxia (CH), and intermittent hypoxia (IH) on true 3D angiogenesis.

3.3 Materials and Methods

3.3.1 Design and microfabrication of microfluidic device

The microfluidic device design has three parallel chambers connected through capillary burst valves measuring 30 μm wide and 100 μm high to facilitate communication between chambers (Fig. 3. 1A). The central compartment (vascular chamber) is the largest with a volume of 0.06 mm^3 (1.5 mm x 0.4 mm x 0.1 mm), and the two adjacent chambers are smaller with a volume of 0.02 mm^3 (0.8 mm x 0.25 mm x 0.1 mm). Only the central compartment has media lines that are connected through capillary burst valves on each end. This design allows for separate chambers to contain different compositions of cells and extracellular matrix as well as to be loaded into the device at different time points. The two media lines were designed to control the flow of media via a difference in hydrostatic pressure head between the two lines. The flow was controlled to mimic physiological fluid velocities of approximately 1-10 μm s^{-1}. Lastly, microfluidic channels adjacent to each of the smaller tissue chambers are present and are used to deliver the oxygen

scavenger to create the oxygen gradient. The microfluidic device design has three parallel chambers connected through capillary burst valves measuring 30 μm wide and 100 μm high to facilitate communication between chambers (Fig. 3. 1A). The central compartment (vascular chamber) is the largest with a volume of 0.06 mm^3 (1.5 mm x 0.4 mm x 0.1 mm), and the two adjacent chambers are smaller with a volume of 0.02 mm^3 (0.8 mm x 0.25 mm x 0.1 mm). Only the central compartment has media lines that are connected through capillary burst valves on each end. This design allows for separate chambers to contain different compositions of cells and extracellular matrix as well as to be loaded into the device at different time points. The two media lines were designed to control the flow of media via a difference in hydrostatic pressure head between the two lines (Fig. 3. 1B). The flow was controlled to mimic physiological fluid velocities of approximately 1-10 μm s^{-1}. Lastly, microfluidic channels adjacent to each of the smaller tissue chambers are present and are used to deliver the oxygen scavenger to create the oxygen gradient.

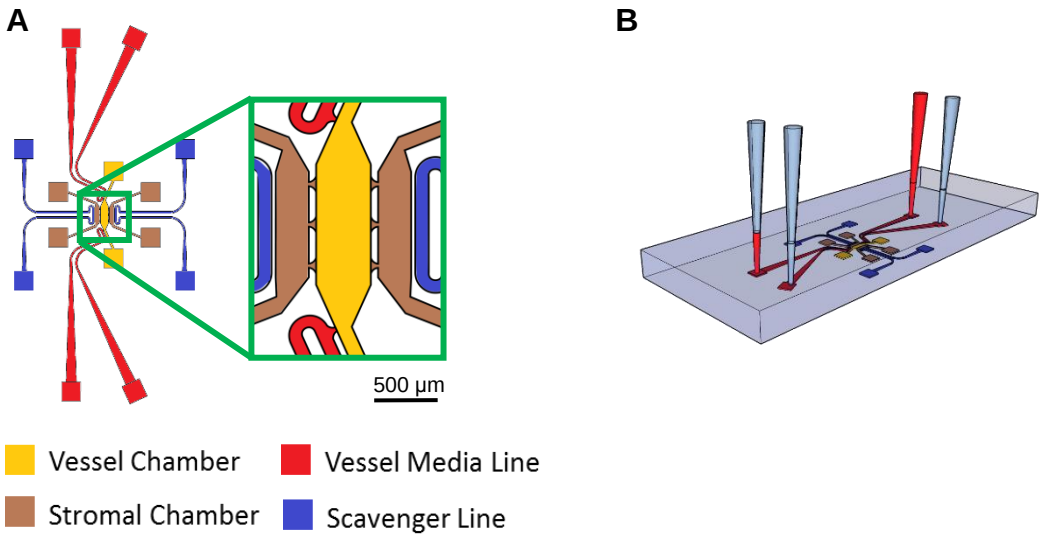

Fig. 3. 1 Microfluidic Device Schematic. (A) The design of the microfluidic device with the central vascular chamber (yellow) and adjacent stromal chambers (brown). Scavenger channels (blue) are placed next to the stromal chambers and media lines (red) feed the vascular chamber. (B) Experimental setup for the microfluidic devices. A difference in hydrostatic pressure head between the inlet and outlet of each microfluidic line creates a drop in pressure between the two sides of the vascular chamber to induce convective interstitial flow throughout the device.

Once a computer-aided design (CAD) of the device was created, the design was printed and standard photolithography methods were used to build the device. Briefly, a negative photoresist, SU-8 3050, (MicroChem, Newton, MA) was spun onto a silicon wafer to a height of 100 μm. Ultraviolet light exposure crosslinked the pattern of the device into the photoresist. After the pattern on the wafer was developed, the mold was silanized and polydimethylsiloxane (PDMS; Dow Corning, Elizabethtown, KY) was poured over the mold at a mixture of 10:1 (w/w) polymer to curing agent. The PDMS was cured in a 65 °C oven overnight. The PDMS was then peeled off the mold and the inlet and outlet holes were punched into the device using an 18 gauge needle for the tissue chambers and 16 gauge needle for the media and scavenger lines. To bond the PDMS device to a glass slide, both pieces were first cleaned to remove debris and then plasma treated for 1 minute at 250 mTorr. After plasma treatment, the PDMS device was sealed to the glass slide and placed in a 120 °C oven for a minimum of 15 minutes. Lastly, the device was sterilized with ultraviolet light before experimentation.

3.3.2 Numerical Simulations

To enhance our understanding of interstitial flow and oxygen concentrations within the device, we created a computational model of mass and momentum transport using COMSOL Multiphysics® 5.2a (Burlington, MA) combined with the CAD model of the device. To simulate the flow throughout the device, a 3D steady state solution of the incompressible Navier-Stokes equations was calculated using no slip boundary conditions for all the walls. Properties of the components of the device are listed in Table 3. 1 and are consistent with previous work. The *transport of diluted species* module was used to model the oxygen gradients throughout the device. Initial conditions for oxygen concentrations was set to 5% O_2. Using Henry's law, the outer boundaries of the device (PDMS-air interface) were set using the incubator level of 5% O_2,

and a Michaelis-Menten kinetic equation was used to simulate cellular metabolism of oxygen.[47] The PDMS-media interface was modeled using a pointwise constraint at the boundary in accordance with the stiff-spring method.[48] A media/PDMS partition coefficient of 0.18 was used in the model. The consumption of oxygen through the reaction with sodium sulfite (Na_2SO_3) was used from previously reported findings in the literature.[47,49–54] In brief, 1 mole of oxygen (O_2) reacts with 2 moles of sodium sulfite (Na_2SO_3) to produce 2 moles of sodium sulfate (Na_2SO_4) with a reaction rate constant, k (Table 3. 1):

$$2Na_2SO_3 + O_2 \xrightarrow{k} 2Na_2SO_4 \qquad \text{(Eq. 1)}$$

Parameter	Value	Unit	Source
Inlet pressure (high side)	25	mmH_2O	-
Outlet pressure (high side)	0	mmH_2O	-
Inlet pressure (low side)	10	mmH_2O	-
Outlet pressure (low side)	0	mmH_2O	-
Fibrin permeability	1.5E-13	m^2	22
Diffusion of oxygen through PDMS	3.55E-9	$m^2\ s^{-1}$	25
Max rate of oxygen metabolism by cells (V_{max})	1.3E-17	$mol\ s^{-1}$	18
Oxygen consumption at half of V_{max} (K_M)	.008	$mol\ m^{-3}$	18
Reaction rate constant (k)	5.77E-5	$M^{0.35}\ s^{-1}$	24
Partition coefficient	0.18	-	19

Table 3. 1 List of Model Parameters.

Opposite the oxygen scavenging channel is a channel open to the atmosphere of the incubator, and thus set to 5% O_2. The computational mesh of the model consists of 700,000-1,000,000 tetrahedral grid elements. For the intermittent hypoxia simulations, time dependent simulations were used with hour cycles of flowing and stopping the reaction with sodium sulfite. To

demonstrate the ability of the device to manipulate the gradient and oxygen tension, additional conditions were modeled to create several unique oxygen profiles. The simulated conditions (Table 3. 2) include modifying the constant chronic hypoxia condition (CH) to having a reduced mass flow rate of the scavenger in the device (rCH), increased wall thickness between the scavenger channel and tissue chambers (wCH), and two scavenging lines (2CH). These modifications were added to demonstrate the versatility of oxygen gradients available with our device.

Condition	**Mass Flow Rate (mol s^{-1})**	**Wall Thickness (μm)**	**Number of Active Scavenger Lines**	**Frequency (h^{-1})**	**Time during cycle (min)**
N	0	-	0	-	Constant
IH_{on}	2×10^{-6}	30	1	0.5	60
IH_{off}	2×10^{-6}	30	1	0.5	60
CH	0.7×10^{-6}	30	1	-	Constant
rCH	0.07×10^{-6}	30	1	-	Constant
wCH	0.7×10^{-6}	60	1	-	Constant
2CH	0.7×10^{-6}	30	2	-	Constant

Table 3. 2 List of Experimental Conditions. N: Normoxia; IHon: Intermittent hypoxia while 2 x 10-6 mol s-1 Na2SO3 is flowing for an hour; IHoff: Intermittent hypoxia while scavenger stopped flowing for an hour; CH: Constant chronic hypoxia of flowing 0.7 x 10-6 mol s-1 Na2SO3; rCH: Constant reduced mass flow rate of oxygen scavenger flowing at 1/10th the speed of CH; wCH: Constant hypoxia with increased thickness of the PDMS wall between the scavenging channel and tissue chamber; 2CH: Constant hypoxia with two active scavenger line

3.3.3 Oxygen Measurements

To validate the oxygen concentration predictions from the computational model, we used phosphorescent lifetime imaging microscopy (PhLIM) that utilizes an oxygen sensitive dye, Oxyphor G4 (Oxygen Enterprises, Philadelphia, PA).[31,55] This Pd-tetrabenzoporphyrin based dye is based on phosphorescence quenching, and we have already demonstrated its proficiency in an *in vivo* model.[56] To excite the phosphorescent dye, we used a 635 nm laser to modulate at 1 kHz with 5% duty cycle (FV1200 Olympus confocal with ISS (Urbana-Champagne, IL) phosphorescent lifetime instrumentation upgrade). The emission beam was collected through a

miniTDU that was equipped with two Hamamatsu 7422p-50 detectors, which was coupled directly to the confocal head. To perform the oxygen measurement, the dye was added to the media of the device at a concentration of 20 μM after the end of the cellular experiment. The dye was allowed to equilibrate for at least an hour through the fibrin and tissue in the device. Oxygen measurements were made over the entire area of the three chambers for each of the three experimental conditions. The phosphorescent lifetime of each pixel was calculated and was then converted into oxygen tension using a previously determined calibration curve at 22 ^{o}C. [31] The advantage of using the PhLIM technique with Oxyphor G4 is that experimental measurements at high spatial and temporal resolution can be achieved.

3.3.4 Cell Culture

As previously described by our lab [57,58], endothelial colony forming cell-derived endothelial cells (ECFC-EC) were derived from cord blood and seeded on 1% gelatin-coated (Sigma-Aldrich, St. Louis, MO) flasks and provided with endothelial growth medium-2 (EGM-2; Lonza, Wakersfield, MD). Normal human lung fibroblasts (NHLF) were commercially purchased and grown in fibroblast growth media (FGM-2, Lonza) before use in the experiments. All cells were cultured in a humidified incubator at 37 °C, 5% CO_2, and 20% O_2 before loaded into the microfluidic device.

To study angiogenesis in the presence of spatial oxygen gradients, transduced ECFC-ECs that constitutively express fluorescence were used to continuously monitor growth of new blood vessels. To transduce the cells, we used a lentiviral particle titer from a human embryonic kidney primary cell line (HEK293T Cells, ATCC, Manassas, VA). The HEK293T cells were seeded in a 6 well plate at a density of 5.0 x 10^5 cells/well and incubated for 24 hours in Dulbecco's Modified Eagle Medium (DMEM, ThermoFisher, Waltham, MA) containing 10% fetal bovine

serum (FBS, Sigma-Aldrich, St. Louis, MO) and no antibiotics. A solution of 250 μL of Opti MEM (Invitrogen, Carlsbad, CA), 7.5 μL of Lipofectamine 2000, and 3μg of plasmid DNA (1.5 μg pLVX-Azurite, .75 μg pMDLg/pRRE, .3 μg pRSV-Rev, and .45 μg pMD2.G) was mixed and incubated for 25 minutes at room temperature. Then, 500 μL of the solution was added dropwise to the wells of the HEK293T cells. The contents of each well was replaced with fresh media 24 hours later. After 48 hours of incubation, the viral supernantant was collected and spun down to exclude cell debris and stored at -80 °C. A T-150 flask of ECFC-ECs were seeded and grown until about 30-40% confluency. Then, a 25 mL solution of EGM containing 8 μg/mL polybrene (Santa Cruz Biotechnology, Dallas, TX) and 500 μL of viral titer was added to the cells and allowed to incubate for 24 hours at 37 °C. The contents of the flask were then aspirated and fresh EGM was added. Transduction efficiency was measured to be more than 90%.

3.3.5 Device Experimentation

For the vascular chamber, ECFC-ECs and NHLFs were trypsinized and resuspended in 16 mg mL^{-1} bovine fibrinogen (Sigma-Aldrich, St. Louis, MO) dissolved in Dulbecco's Phosphate Buffered Saline (DPBS; ThermoFisher). The ECFC-ECs were collected at 5 x 10^6 cells mL^{-1} and the NHLFs were collected at 10 x 10^6 cells mL^{-1}. Thrombin (Sigma-Aldrich) was prepared to a concentration of 50 U mL^{-1} in DPBS and added to the cell-fibrinogen solution. This initiated the polymerization process, and the solution was quickly pipetted into the central or vascular chamber of the device. After incubating the gel for 30 minutes at 37 °C, EGM-2 was added to the media lines for the first 24 hours of the experiment and flow was maintained using a hydrostatic pressure head. Afterwards, the devices were placed in a 37 °C, 5% CO_2, and 5% O_2 incubator and EGM-2 without growth factors was used to feed the tissue. The direction of the pressure

gradient throughout the device was switched every day to ensure spatially homogenous growth.[59,60]

Following the first four days of the experiment, vascular structures were apparent, and the adjacent chambers were then loaded with fibroblasts in a fibrin gel at a concentration of 7.5×10^6 cells mL^{-1} using the previously described method. After 24 hours, the oxygen scavenger, sodium sulfite (Sigma Aldrich, St. Louis, MO), was dissolved in deionized water and pushed through the left scavenger channel of the device using a syringe pump. Only one of the scavenging channels had an oxygen scavenger flowed through it. The other channel (farthest right channel) was kept open to atmosphere to keep the right tissue chamber close to normoxia. Tygon tubing (Saint-Gobain, Valley Forge, PA) was used to connect the sodium sulfite syringes with the devices. To ensure that the two hypoxia conditions had the same average oxygen concentration over the duration of the experiment, 0.35M sodium sulfite was flowed at 120 µl min^{-1} (mass flow rate of 0.7×10^{-6} mol s^{-1}) continuously for the CH condition while 1 M flowed at 120 µl min^{-1} (mass flow rate of 2×10^{-6} mol s^{-1}) was used for the IH condition with the pump programed for 1 hour of scavenger flow (IH_{on}) and 1 hour of no flow (IH_{off}). To mimic CH and IH, sodium sulfite was introduced through the left side of scavenger line for 6 more days until the end of the duration of the experiment. Because sodium sulfite constantly reacts with oxygen, it was important to maintain a constant flow of oxygen scavenger.

3.3.6 Quantification of Biased Angiogenesis

At the end of the experiment, images were taken of the fluorescent vascular network in each of the chambers. To quantify sprouting angiogenesis, images were cropped to only contain the left or right stromal chamber. The images were randomized and blinded for image analysis in

ImageJ. Multiple devices were used for each condition of N (n=8), CH (n=11), and IH (n=17). We calculated biased angiogenesis using the following relationship:

$$\text{Biased Angiogenesis} = \frac{\text{Vessel area in left or right chamber}}{\text{Vessel area in left chamber+vessel area in right chamber}} \quad \text{(Eq. 2)}$$

In other words, the vessel area in each side chamber is expressed as the fraction of total angiogenesis into both chambers. A value of 0.5 indicates unbiased angiogenesis.

3.3.7 Statistical Analysis

Because the data was not normally distributed, the parameters are presented with medians and ranges from the 25% to 75% percentile. To determine if the biased angiogenesis and vessel area in the left chamber was significantly different compared to the right chamber, a nonparametric Mann-Whitney test was applied using GraphPad Prism. Significance was determined at the $p < 0.05$ level.

3.4 Results

3.4.1 Microfluidic Device: Pressure and Flow

After successful construction of the microfluidic device, we demonstrated desired pressure and velocity profiles (Fig. 3. 2A-B). The steady pressure profile of the device (Fig. 3. 2A) demonstrates a drop in pressure in the vascular chamber to the stromal chambers from 1×10^{-2} mmH_2O to 0.5×10^{-2} mmH_2O (approximately 9.8×10^{-2} to 4.9×10^{-2} Pa), respectively, with the stromal chamber averaging 0.85×10^{-2} mmH_2O (8.3×10^{-2} Pa). Additionally, the device was designed to create physiologically relevant fluid velocities ranging between 1-10 $\mu m\ s^{-1}$ by appropriately adjusting the hydrostatic pressure head (25 mmH_2O, Fig. 3. 2). Another design consideration to note is that the adjacent stromal chambers do not have separate media lines; the chambers receive nutrients through the vascular chamber as shown by the streamlines (Fig. 3.

2B). To demonstrate this effect in the device, fluorescein isothiocyanate-dextran (FITC-dextran) was introduced through the media lines to show the direction of fluid flow through the connecting pores (Fig. 3. 2C).

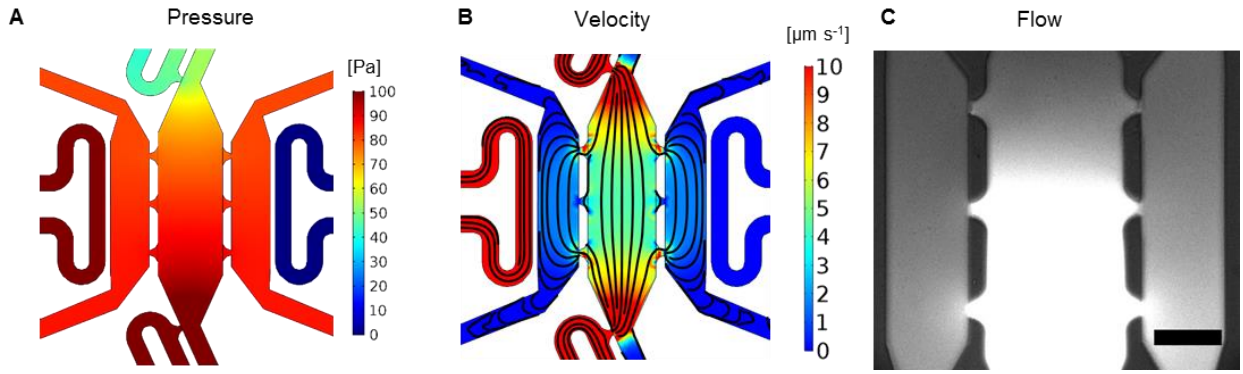

Fig. 3. 2 Microfluidic Device Characterization. (A) Surface map of the steady pressure (Pa) distributions inside the microfluidic device. (B) Surface map of the fluid velocity (μm s^{-1}) and streamlines. (C) FITC-dextran was introduced through the media lines to demonstrate the direction of flow through the device (bottom to top and central chamber to outside chambers). The image was taken 30 minutes after introducing the dye. Scale bar = 200 μm.

center). In addition, a horizontal line (represented by a white arrow) was drawn in the middle of the chambers to quantify the gradient across the device (Fig. 3. 3A-C, top row). With no scavenger present (N condition) the oxygen concentration remains constant near 5% O_2 throughout the device (Fig. 3. 3A, top, and Fig. 3. 3E). Although the device is fairly symmetric, the placement of the media lines on the left side of the central chamber (Fig. 3. 1A) raises oxygen tension slightly in the left stromal chamber. The CH condition (0.7 x 10^{-6} mol s^{-1} sodium sulfite) created a steady state oxygen gradient from 3.2% O_2 in the left chamber to 4.6% O_2 in the right chamber (Fig. 3. 3B, top, and Fig. 3. 3E), and a mean concentration of 4% O_2 in the central chamber.

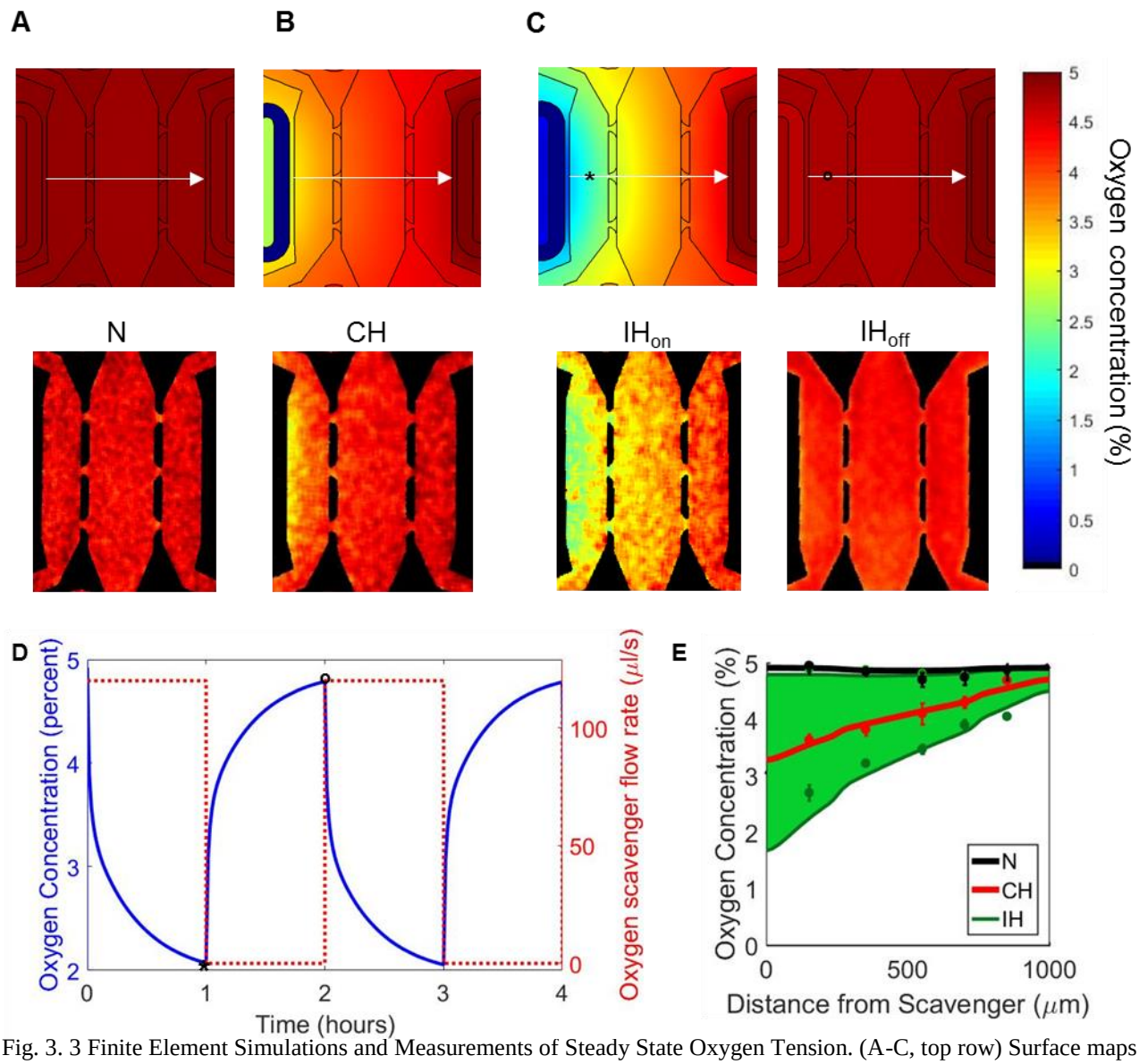

Fig. 3. 3 Finite Element Simulations and Measurements of Steady State Oxygen Tension. (A-C, top row) Surface maps of theoretical oxygen tension in different conditions are shown. (A) Normoxic condition (N) with no oxygen scavenger, (B) constant chronic hypoxia condition (CH) with a constant flow of 0.35 M sodium sulfite flowing at 120 µl min^{-1}, and (C) intermittent hypoxia (IH) condition of alternating 1 M sodium sulfite flowing at 120 µl min^{-1} for an hour (IH$_{on}$, left panel) and no flow of oxygen scavenger for an hour (IH$_{off}$, right panel). (A-C, bottom) Experimental oxygen maps were constructed using a PhLIM technique for the N (A, bottom), CH (B, bottom), and IH (C, bottom) conditions. The IH$_{on}$ measurements were taken an hour after flowing sodium sulfite, and the IH$_{off}$ measurements were taken an hour after stopping flow. (D) Temporal variations of the oxygen tension at a point in the left stromal chamber from the COMSOL model in (C, top). The asterisks (*) and circle (o) on the oxygen maps corresponds to the low and high points of the graph, respectively. (E) Comparing the oxygen profiles of all the varying conditions along the central line of the three chambers (arrow in A-C). The conditions are N (black), CH (red), IH (green). The IH case is represented by a green area to illustrate the range of oxygen profiles between the two extreme states of the condition. The solid lines are values from the COMSOL model, and the points are averages from the PhLIM measurements for the three conditions (n=3 for each conditions).

The IH condition was designed to have the same average oxygen concentration over time as CH. After one hour of 2 x 10^{-6} mol s^{-1} sodium sulfite flowing through the scavenger line in the IH condition, the oxygen tension ranged from 1.7% (left) to 4.5% (right) O_2 (Fig. 3. 3C, top left, and Fig. 3. 3E). After one hour of no scavenger flow, the oxygen profile resembled the normoxia case with the average concentration being only slightly less than 5% O_2 (Fig. 3. 3C, top right, and Fig. 3. 3E). The time averaged mean concentration in the central chamber over a complete cycle was 4% O_2, similar to that of CH. The temporal variations of a fixed position in the middle of the left chamber is shown by the * and o symbols in Fig. 3. 3C to demonstrate the dynamics in our device (Fig. 3. 3D). This figure also shows the step function of the flow of oxygen scavenger going from 120 μl min^{-1} to no flow. Although the sodium sulfite reacts with oxygen quickly to lower the concentration, there is a lag to reach the final oxygen concentration (Fig. 3. 3D). In these experiments, we used molar concentrations of sodium sulfite to ensure a zero concentration of oxygen within the solution. The reaction of sodium sulfite depends only on the concentration of sodium sulfite and is zero order with respect to oxygen[53]; thus, the aqueous solution of sodium sulfite quickly (minutes) depletes all the oxygen before entering the microfluidic device. This makes sodium sulfite a very effective solution for creating hypoxic oxygen gradients.

Experimental oxygen measurements were taken once the dye reached equilibrium within the device. The oxygen maps of the experimental conditions are shown in Fig. 3. 3A-C, bottom, with the measurements for the intermittent hypoxia condition taken one hour after each cycle began. The experimental oxygen concentrations (mean top to bottom for each location from the scavenger) for each condition (Fig. 3. 3E) were in agreement with the simulated values (Fig. 3. 3A-C, top row).

To illustrate the utility of the microfluidic device for different spatial and temporal oxygen gradients, we performed three additional simulations (Table 3. 2, Fig. 3. 4). The first condition, rCH, consisted of reducing the mass flow rate of sodium sulfite to 1/10th the original speed compared to CH (0.07 mol s^{-1}, Fig. 3. 4A) which increases the oxygen concentration (range of 4.5% to 4.9% O_2). Next, the condition wCH manipulated the oxygen profile by changing the thickness of the PDMS wall that separates the tissue chambers and the scavenger line. By doubling this wall to 60 μm compared to CH (wall thickness of 30 μm), and using the original mass flow rate of 0.7 x 10^{-6} mol s^{-1}, the overall concentration of oxygen was also increased (range of 3.4% to 4.7% O_2, Fig. 3. 4B). Lastly, the condition 2CH drastically changed the oxygen profile by flowing 0.7 x 10^{-6} mol s^{-1} sodium sulfite through both scavenger lines. This condition lowered the overall concentration of oxygen in the device by scavenging both sides. In contrast to all previous simulations, the middle chamber had the highest oxygen concentration as it was the furthest from the scavenger lines. The oxygen tension range in this case was 2.4% to 2.8% O_2 (Fig. 3. 4C). The oxygen quantification of each condition is shown in Fig. 3. 4D and represents the concentration of oxygen at each distance along the middle of the chamber (arrow in Fig. 3. 4A-C). As with the previous simulations, because of the subtle asymmetry of the device, the oxygen gradient is not perfectly symmetric although the two scavenger lines have the same mass flow rate of sodium sulfite. The simulations show a range of oxygen tensions that can be achieved by varying parameters such as oxygen scavenger concentration, time exposed to an oxygen scavenger, flow rate of the oxygen scavenger, membrane wall thickness, and number of active scavenger lines.

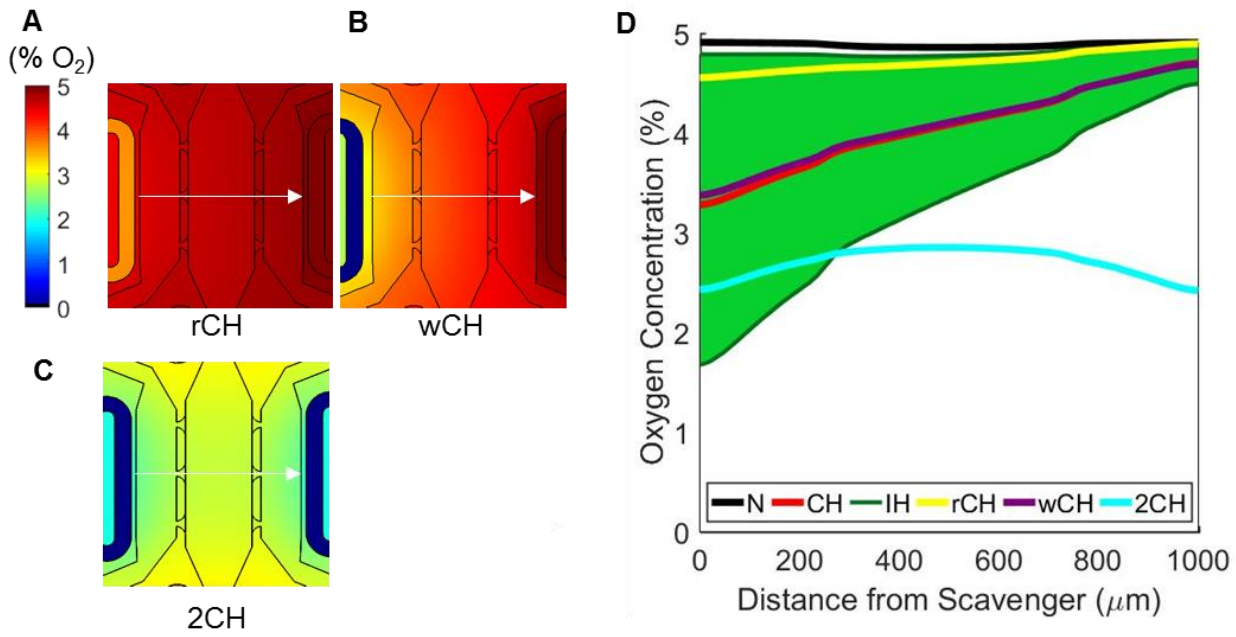

Fig. 3. 4 Varying Device Parameters. (A) Reduced mass flow rate condition (rCH) with 0.07 x 10^{-6} mol s^{-1} of sodium sulfite. (B) Increased wall distance (wCH) between the scavenger channel and stromal chamber to 60 µm. (C) Two active scavenger lines (2CH). (D) Comparing the oxygen profiles of all the varying conditions along the central line of the three chambers (arrow in A-C) with the experimental conditions from Fig. 3. The conditions are N (black), CH (red), IH (green), rCH (yellow), wCH (purple), and 2CH (blue).

3.4.3 Angiogenesis within the three-chambered device

The ECFC-ECs and NHLFs in the central chamber were allowed to grow in a fibrin gel independently for the first four days of the experiment until early vasculature structures were apparent. On day 4, NHLFs in a fibrin gel were loaded into the adjacent left and right chambers, and after 24 hours of incubation, the NHLFs began to spread and resume normal fibroblast morphology. Sprouting vasculature into the left and right stromal chambers was apparent after 6 days.

At the end of the experiment, each condition had devices that sprouted vessels into the adjacent chambers. Fig. 3. 5A shows representative images of the three conditions at the start (left panels) and end (right panels) of the experiment. After images of the left and right chambers were randomized and blinded for image analysis, parameters of vessel area and angiogenesis bias were

calculated. In the N condition, the left chamber had an average area of 35,577 (8,034 – 46,742) μm^2 and the right chamber had an average area of 40,582 (10,109 – 62,537) μm^2. This generated values for angiogenesis bias of 0.45 (0.18 – 0.65) and 0.55 (0.35 – 0.82) for the left and right chambers, respectively, which were not statistically significant. In the CH condition, the left chamber had an average area of 12,606 (1,644 – 14,696) μm^2, which was significantly higher than the right chamber with an average area of 1,187 (167 – 2767) μm^2, $p < 0.05$. This result was also present in the angiogenesis bias for the left and right chambers which were 0.93 (0.72 – 1.0) and 0.07 (0.0 – 0.28) respectively ($p < .0001$). Lastly, the IH case also had significantly different vessel areas in the adjacent chambers with the left chamber having an average of 4,664 (3,121 – 6539) μm^2 and the right chamber having an average area of 1,289 (300 – 4970) μm^2, $p < 0.05$. This trend produced an angiogenesis bias of 0.78 (0.51 – 0.96) and 0.22 (0.04 – 0.49) for the left and right chambers which was statistically significant ($p < .0005$) (Fig. 3. 5B-C).

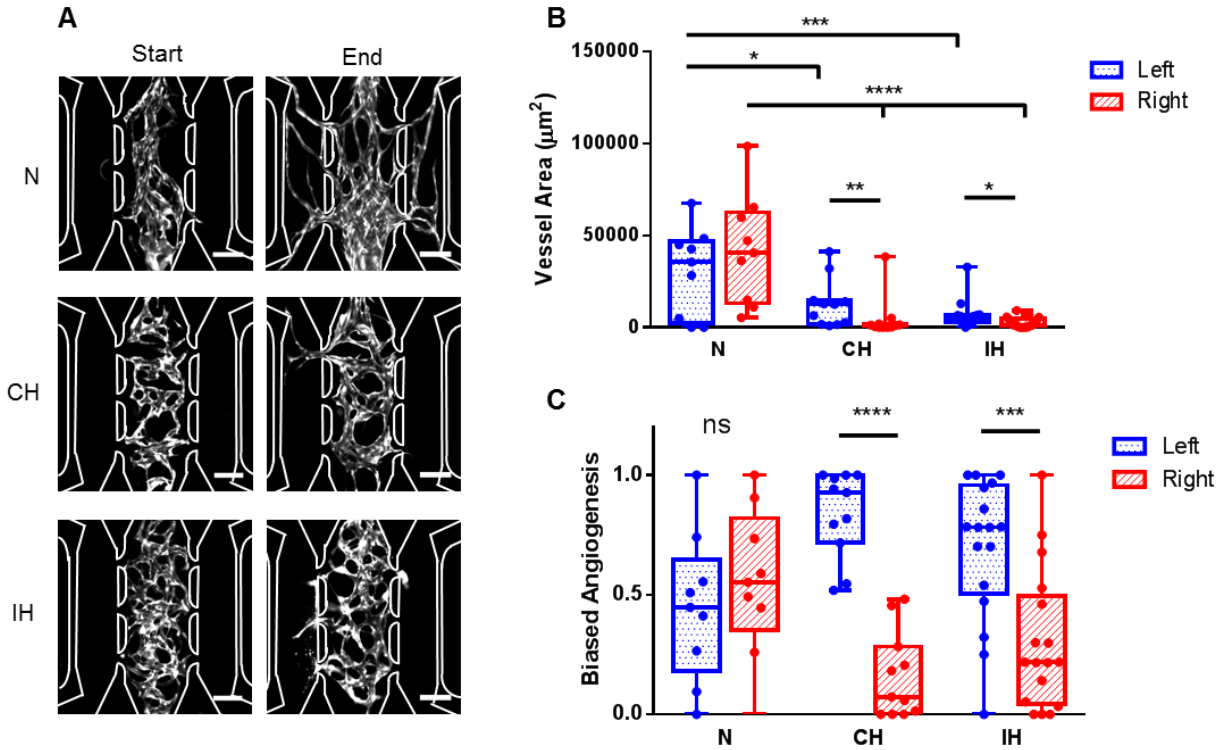

Fig. 3. 5 Biased Angiogenesis Due to Hypoxia. (A) Representative images from the N (top), CH (middle), and IH (bottom) conditions. In each category, images of the vascular network before (left) and after (right) the condition was applied is shown. (B) The total vessel area for each category in the left and right stromal chambers were measured and compared. For both hypoxic conditions, the vessel area in the left stromal chamber (closer to the scavenger channel) was significantly higher than the right chamber. (C) Biased angiogenesis was calculated for the left and right stromal chambers in each condition and compared to each other. Both hypoxic conditions had significantly more bias in the left stromal chamber. N, n=8; CH, n=11; IH, n=17. Scale bar = 200μm * p<.05, ** p<.005, *** p<.0005, **** p<.0001.

We also created control conditions that contained no fibroblasts in the adjacent compartments (plain fibrin) under normoxic and constant chronic hypoxic conditions. In the normoxic case, there were no angiogenic sprouts into the adjacent chambers. On the other hand, the device with plain fibrin in the adjacent chambers had degraded vessels under the constant chronic hypoxic condition (data not shown).

3.5 Discussion

A promising use of organ-on-a-chip technology is the ability to mimic and test disease states. Hypoxia is a prominent feature of diseases such as wound healing, ischemia, and cancer. Hence, the ability to control oxygen within a microfluidic device provides a unique opportunity to understand the impact of oxygen tension at high spatial and temporal resolution. While common previous studies may set an incubator to a specific oxygen concentration, this does not create the oxygen concentration gradients that are relevant to human physiology. The structure of the microcirculation is sensitive to oxygen tension, and our device design demonstrates the ability to spatially (microns) and temporally (minutes) control the oxygen concentration around a steady vascular network to study these effects. Our device can introduce various combinations of cells and extracellular matrix at different time points as well as manipulate the oxygen concentration to simultaneously compare the effects of a normoxic and hypoxic stromal chamber on a neighboring vascular network.

Our ability to experimentally measure oxygen within the device provides the opportunity to validate the performance and accuracy of the platform and model simulations. PhLIM provides high spatial resolution in 3D that is capable of capturing an entire oxygen map. This is a distinct advantage over traditional oxygen sensors and probes that are placed on one surface or in a single position and rely on models to extrapolate the3D oxygen map. The PhLIM oxygen measurements closely match the oxygen values predicted by the model over a range of experimental conditions.

While other intermittent hypoxia studies typically switch between 20% and 1% O_2 [42–44], it is physiologically more relevant to cycle between 5% and 1% O_2 to replicate disease states such as the tumor microenvironment in the presence of leaky vasculature.[10] In our simulations and experiments, we are able to easily produce oxygen values in the 1-5% O_2 range. Although we only tested one frequency in this study, our device has the ability to recreate longer or more extreme hypoxic frequencies. While other studies have found results that may suggest that intermittent hypoxia can increase proliferation or migration of fibroblasts, these studies often cycle between 20% O_2 and 1% O_2.[61] Even though we did not see these results in our intermittent hypoxia condition, we believe that our results are more relevant to human physiology because we chose to cycle between oxygen concentrations that are apparent *in vivo*.

To demonstrate the biological relevance of our device, we investigated the ability of constant chronic and intermittent hypoxia to stimulate angiogenesis. In normoxia (5% O_2), vessel growth was relatively uniform into both adjacent tissue compartments. Although not statistically different, small variances between the left and right compartments could be due to the slight asymmetry in the design. Our device was able to recreate sprouting angiogenesis into a hypoxic tissue microenvironment under both constant chronic and intermittent conditions. This

observation is consistent with a normal biological response.[25,61,62] The hypoxic conditions generated less total vasculature than the normoxia case. This can be explained by the lower mean oxygen tension within the vasculature chamber of the CH and IH cases (as low as 3.5% and 2.5%, respectively, compared to 5%). The lower oxygen tension in the two hypoxic conditions likely results in hypoxic stress to the vascular network and reduced overall sprouting.

The constant chronic hypoxia condition had more significant angiogenesis bias towards the low oxygen chamber compared to the intermittent hypoxia condition as well as greater vessel area. This is probably due to the range of oxygen concentrations we've chosen as well as frequency of the cycle. Alternatively, as the constant chronic hypoxia case is a continuous exposure to hypoxia, the stressed fibroblasts in the left chamber might have continually expressed pro-angiogenesis factors to encourage more vessel growth relative to the intermittent hypoxia condition. As shown previously by our group, the frequency of the intermittent hypoxia cycles can change how a vessel responds, which can be correlated to the amount of vascular endothelial growth factor that is secreted by hypoxic fibroblasts.[63]

3.6 Conclusion

The results of this study show the effectiveness of microfluidic devices to control and manipulate oxygen tension at high spatial and temporal resolution. The device design demonstrates the ability to load different types of cells at different time points, which provides the opportunity to model many different normal and pathological states. We chose 3D sprouting angiogenesis to demonstrate the biological relevance of the device design, and we were able to replicate the well-described angiogenic response of hypoxic (constant chronic and intermittent) fibroblasts. The simple and flexible design of the devices provides an opportunity to enhance understanding of important disease processes present in cancer, ischemic heart disease, and wound healing.

Chapter 4: Knockdown of HIF-1α Affects MDA-MB-231 Survival under Spatial and Temporal Oxygen Gradients

4.1 Abstract

The cost of guiding a clinical drug through discovery and development has been on the rise, and it is now estimated that one drug can cost as much as $1.3 to $2.6 billion dollars. One method to reduce costs is to create better platforms that more accurately replicates human disease physiology in the pre-clinical phase to improve the efficiency and success in the clinical trial phase. As cancer is the second leading cause of death in America, the development of new therapies remain a priority. It been shown that tumor hypoxia, or low oxygen tension, contributes to cancer drug resistance, yet most experiments mimicking cancer drug response are done at atmospheric oxygen concentration (20% O_2). This condition is a poor representation of hypoxic tumor biology *in vivo* (< 5% O_2). Furthermore, the leaky and tortuous nature of tumor vasculature contributes to an oxygen tension that can fluctuate temporally between hypoxia and normoxia (5% O_2), a condition known as intermittent hypoxia. To replicate these dynamics of the tumor microenvironment, we have designed a microfluidic device that can control the spatial and temporal gradients of oxygen using an oxygen scavenger, sodium sulfite, to create an oxygen sink. The scavenger is placed in microfluidic line next to a tissue chamber that contains MDA-MB-231 breast cancer cells grown in a fibrin gel. Finite element modeling were used to predict the oxygen gradients achieved in the microfluidic device. We knocked down the expression of hypoxia inducible factor 1 alpha, the key transcriptional regulator of hypoxia and a common therapeutic target of tumor hypoxia, to understand how the tumor cells would survive in an

oxygen gradient. We found that both the oxygen concentration and the duration spent at hypoxia are critical determinants of tumor cell migration and survival. This study demonstrates that both spatial and temporal dynamics of oxygen tension in the tumor microenvironment could impact drug efficacy.

4.2 Introduction

Hypoxia, or low oxygen tension, has become a hallmark of tumor progression as tumor cell proliferation commonly exceeds diffusion of oxygen from the local vascular network creating an imbalance of supply and demand. Furthermore, clinical studies showed advanced breast cancer having a lower oxygen tension (10 mmHg) than normal breast tissue (65 mmHg).[10] Subsequently, hypoxia has been associated with poor patient prognosis due to gene expression changes that tumor cells can undergo during this process. Some processes associated with tumor hypoxia are migration, tumor angiogenesis, metabolic reprogramming, cancer stem cell maintenance, dormancy, and immune evasion, all which can contribute to treatment resistance.[64,65] In addition, the heterogeneity of vasculature in the tumor microenvironment can lead to instances of intermittent hypoxia of repeated oxygen tension < 5% O_2 cycling with normoxia. Nevertheless, both chronic (sustained oxygen tension < 5% O_2) and intermittent hypoxia have been shown to contribute to tumor progression.

Tumor response to hypoxia is controlled largely by the transcription factor hypoxia-inducible factor 1 (HIF-1).[22,66] HIF-1 has two subunits (HIF-1α and HIF-1β), and under normal oxygen conditions, HIF-1α is rapidly degraded by a family of prolyl hydroxylases. However, when as oxygen tension decreases, the action of the prolyl hydroxylases is progressively compromised leading to increased levels of HIF-1α in the cytoplasm. HIF-1α is then free to translocate to the nucleus where it forms a heterodimer with HIF-1β and binds to the hypoxia responsive elements

(HRE) in the promoter region of many genes. For example, increased levels of HIF-1α can lead to enhanced expression of pro-angiogenic factors such as vascular endothelial growth factor (VEGF) and VEGFR1, VEGFR2, plasminogen activator inhibitor-1 (PAI-1), angioprotein-2 (Ang-2), and inducible nitric oxide synthase (iNOS).[10] While it has been established that hypoxia increases expression of HIF-1α, our understanding of how temporal changes in oxygen tension influence HIF-1α is incomplete. Although preliminary data has shown support that cyclic hypoxia may increase the presence of HIF-1α, no direct link has been made to hypoxia cycle duration or magnitude.[67–70] All these studies of various cancer types under intermittent hypoxia showed that an increase in HIF-1α expression lead to tumor progression in terms of increased tumor angiogenesis, metastasis, or increased stem-like properties due to downstream signaling.[67–70]

Because HIF-1α plays such an important role during hypoxic tumor progression, it is a potential target for tumor treatment. However, this has been met with varying success, likely due to our incomplete understanding.[71–73] While most studies have examined the degree of hypoxia[74–76], we hypothesize that temporal variations of oxygen also impact tumor progression. To study this hypothesis, we knocked down HIF-1α in breast cancer MDA-MB-231 cells and applied both spatial and time varying oxygen concentrations. Our results show that both the spatial and temporal gradients of oxygen affect tumor survival and migration of MDA-MB-231, and that this response is HIF-1α-dependent.

4.3 Methods

4.3.1 Construction of Microfluidic Device

In this study, we used a three chambered microfluidic device (**Error! Not a valid bookmark self-reference.**). The chambers were connected to each other via capillary burst valves

measuring 30 μm wide. The fibrin chamber (central compartment) is the largest with a volume of 0.06 mm^3, and the adjacent tumor chambers (adjacent) are slightly smaller with a volume of 0.02 mm^3. Media lines connect to the central chamber to feed the adjacent tumor chambers, and interstitial flow is driven by a hydrostatic pressure head. Finally, microfluidic channels 100 μm wide run parallel to the tumor chambers and are used to deliver the oxygen scavenger to the device.

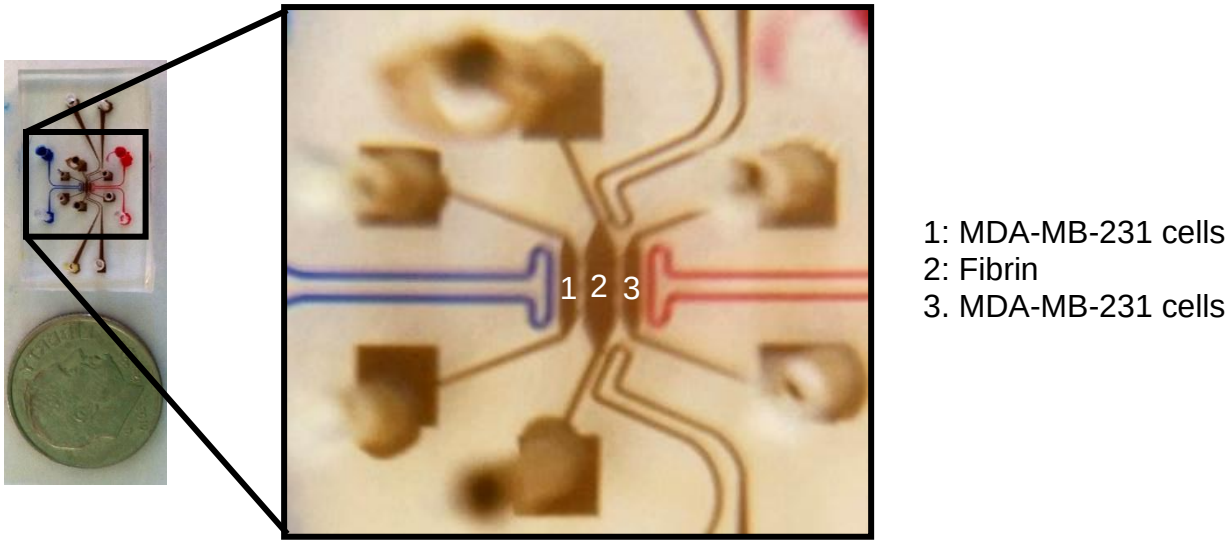

Fig. 4. 1 Device Schematic. Our device is about the size of a US dime (left image). It consists of three tissue chambers (larger brown chambers) and two media lines (smaller brown lines). The outer chambers are loaded with MDA-MB-231 cells in gel, and the central chamber is loaded with plain fibrin. Sodium sulfite is convected through the scavenger line (blue), while the opposite line (red) is left open to atmosphere.

After the device design was created in AutoCAD (San Rafael, CA), the design was printed and fabricated using standard photolithography methods. Briefly, SU-8 3050 (MicroChem, Newton, MA), a negative photoresist, was spun on to a silicon wafer to a height of 100 μm. Using the printed design, ultraviolet light was used to crossline the pattern into the photoresist. Next, a developer was used to leave the crosslinked pattern on the wafer. This mold was then silanized and polydimethylsiloxane (PDMS; Dow Corning, Elizabethtown, KY) was poured over the mold at a mixture of 10:1 (w/w) polymer to curing agent. The polymer was then cured at 65 °C for at

least two hours. The PDMS was then peeled off and the devices were cut individually. The inlets and outlets were punched out of the device using blunt needles. To bond the device to a glass slide, both pieces were cleaned and then plasma treated. Once the device was sealed to the glass, it was placed in a 120 °C oven for a minimum of 15 minutes. Finally, to sterilize the device before experimentation, it was placed under ultraviolet light for 1 hour.

4.3.2 Finite Element Modeling

To understand the oxygen gradients achieved in our microfluidic device, a 3D model of mass and momentum transport was created in COMSOL Multiphysics 5.2a (Burlington, MA). First, understand the delivery of oxygen through the media lines, flow was modeled by solving the steady state solution of the incompressible Navier-Stokes equations using a no slip boundary condition for the walls. The different properties of the device are the same as those used previously (Table 1). The modeling of the 3D oxygen gradients is the same as previously described in Chapter 3.3.2. Briefly, the *transport of diluted species* module was used to mimic the transport of oxygen through the PDMS layer. Michaelis-Meten kinetics was used to model consumption of oxygen via cellular metabolism and the consumption of oxygen through the sodium sulfite reaction was based on previously reported findings in literature.[52]

4.3.3 MDA-MB-231 Cell Culture

Breast cancer cells, MDA-MB-231 cells, were purchased for this study from Cell Biolabs, Inc. (San Diego, CA) and grown in Dulbecco's Modified Eagle Medium (DMEM, ThermoFisher, Waltham, MA) containing 10% fetal bovine serum (FBS, Sigma-Aldrich, St. Louis, MO), 1% L-glutamine (ThermoFisher), and 1% penicillin streptomycin (ThermoFisher). Cells were cultured in a humidified incubator at 37 °C, 5% CO_2, and 20% O_2 before loaded into the microfluidic device.

4.3.4 HIF-1α Knockdown in MDA-MB-231

For the scramble and shRNA HIF-1α lentiviral particle transduction (Santa Cruz Biotechnology, Dallas, TX), we first seeded MDA-MB-231 in a 24-well plate at a concentration of 4.5 x 10^4 cells in each well and allowed to grow overnight to about 50% confluency. A 250 µl media solution containing 5 µg mL^{-1} polybrene (Santa Cruz Biotechnology) was added dropwise to each well. Next, a 250 µl solution of media and lentiviral particles at a dilution of 1:50 (v/v) particles to media or a multiplicity of infection (MOI) of about 1 was added to each well. The cells were allowed to incubate with the lentiviral particles for 18 hours before the media was changed. Stable clones expressing the scramble and shRNA lentiviral particles were selected via 3 µg mL^{-1} concentration of puromycin dihydrochloride (Santa Cruz). These cells were then tested for HIF-1α gene expression by qRT-PCR and then frozen.

To perform qRT-PCR, RNA was extracted and purified using the RNeasy Plus Mini Kit (Qiagen, Venlo, Netherlands) to a concentration of 100 ng $µl^{-1}$. A reverse transcription kit (Applied Biosystems) was then used to convert the RNA to cDNA. HIF-1α gene expression was then measured using Taqman Gene Expression Assays (HIF-1α: Hs00154153_m1, 18S: Hs99999901_s1) using the CFX96 Real-Time PCR Detection System (Bio-Rad, Hercules, CA). Relative HIF-1α gene expression for control MDA-MB-231 (Control), scramble MDA-MB-231 (Scramble), and shRNA HIF-1α MDA-MB-231 (shHIF-1α) were compared using the $\Delta\Delta C_t$ method.

4.3.5 Microfluidic Device Experiment

The central chamber was first loaded with fibrin by resuspending 16 mg mL^{-1} fibrinogen (Sigma-Aldrich) in Dubecco's Phosphate Buffered Saline (DPBS, ThermoFisher) and mixing it with a 50 U mL^{-1} thrombin solution. This initiates the polymerization process, at which time the mixture

was quickly pipetted into the central chamber. The gel was then incubated for 30 minutes at 37 °C to ensure the polymerization process was complete. Next, the adjacent chambers were loaded with MDA-MB-231 cells at a concentration of 5 x 10^6 cells mL^{-1}. The cells were mixed with the fibrinogen solution, and then this cell-fibrinogen solution was mixed with thrombin before pipetting it in to the left and right chambers. After complete polymerization of the fibrin gel, DMEM was flown through the media lines connected to the central chamber. The devices were then placed in a humidified incubator at 37 °C, 5% CO_2, and 5% O_2 overnight. The next day, the devices were imaged and the sodium sulfite was added to the left scavenger channel at varying concentrations. This treatment was applied for the next 6 days before stopping the experiment and performing a live/dead stain and imaging the devices.

In this study, we performed 4 different chronic hypoxia (CH) and 2 different intermittent hypoxia (IH) studies. To achieve a range of different oxygen tensions, we varied the sodium sulfite concentrations. In the chronic hypoxia condition, we used 1mM (1CH), 2mM (2CH), 3mM (3CH), and 5mM (5CH) concentrations of sodium sulfite. The solutions were placed in a syringe and tygon tubing (Saint-Gobain, Valley Forge, PA) was used to connect the syringe to the devices. For the duration of the experiment, the solutions were delivered continuously at a rate of 12 μl min^{-1} to maintain constant consumption of oxygen during the entire length of the experiment. Together, the concentration of sodium sulfite and the flow rate of the solution produced a mass flow rate that created a variety of desired oxygen gradients to affect the survival of shHIF-1α cells. The two intermittent hypoxia studies were intended to have the same temporal oxygen concentration average of the 1CH and 3CH conditions and were termed 1IH and 3IH respectively. Based on previous literature, we used a 1:1 ratio of time spent flowing scavenger to time with no scavenger flow.[68,70] To ensure that 1IH had the same temporal oxygen

concentration average as 1CH, we used a concentration of 3mM sodium sulfite and flowed it for a total of 12 hours, before stopping flow for 12 hours. These calculations were based on the reaction kinetics of sodium sulfite. Similarly, in our 3IH condition, we used a sodium sulfite concentration of 9mM, and flowed it for a 1 hour cycle before stopping flow for an hour. Overall, we could test a variety of spatial and temporal oxygen gradients on Control, Scramble, and shHIF-1α cells.

4.3.6 Tumor Growth and Migration Quantification

To quantify the degree of tumor progression in our study, we split up this parameter into two factors: growth and migration. Images of the microfluidic device were taken before hypoxia treatment and at the end of the experiment. Each image was cropped to only contain the left, central, or right chamber, and the images were randomized and analyzed for tumor area using ImageJ. Tumor growth was defined as normalized tumor area (NTA), and is defined by the area in the left or right chamber on the final day of the experiment divided by the same chamber on day 1. The migration parameter we used was calculated by dividing the tumor area in the central chamber by the total tumor area in the left, central, and right chamber on the final day of the experiment.

4.3.7 Statistical Analysis

All conditions were performed using at least 3-6 biological replicates, and the results are represented as mean ± SD. A Mann-Whitney test was applied to compare tumor growth in the left and right chambers or migration parameter among shHIF-1α cells, Control or Scramble. Statistical significance was considered at the $p < 0.05$ level, and GraphPad Prism 6 was used for data analysis.

4.4 Results

4.4.1 Microfluidic Device and Oxygen Concentration Profiles

As we have shown previously, our microfluidic device can produce reliable pressure and velocity gradients to ensure the growth of the tissue inside the device. We were successfully able to observe tumor progression over the seven days of the experiment with the ability to quantify tumor growth as well as tumor migration.

To understand the oxygen gradients we would achieve, we used extensive finite element modeling to predict the oxygen tension within the device (Fig. 4. 2). Various sodium sulfite concentrations were used in the models and demonstrate that by decreasing the concentration of scavenger, there is an attenuation of the oxygen gradient. The 1CH condition has an oxygen concentration rate of 4.93% to 5% O_2. On the other hand, the 5CH condition has an oxygen concentration rate of 4.89% to 5% O_2.

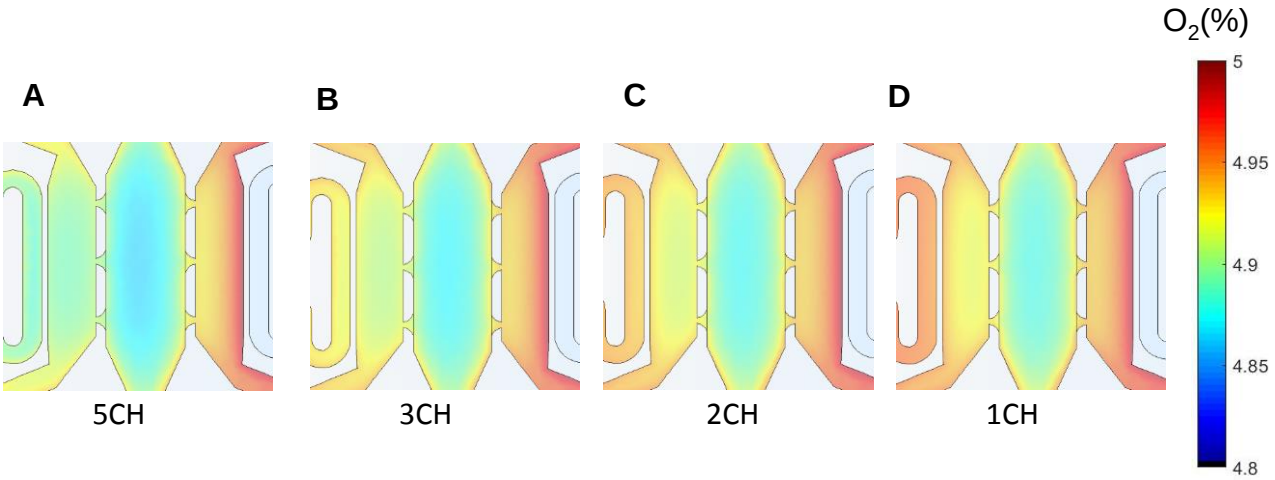

Fig. 4. 2 Model of the oxygen distributions for various sodium sulfite concentrations. (A) 5CH, (B) 3CH, (C) 2CH, and (D) 1CH conditions show that decreasing the concentration of sodium sulfite attenuates the oxygen gradient in the device.

4.4.2 Response of MDA-MB-231 to Varying Oxygen Gradients

The first experiment compared the growth of Control cells grown in 20% O_2 to the more physiologically relevant 5% O_2. We observed significantly more growth in 5% O_2 compared to 20% O_2 (7.461 ± 4.64 NTA compared to 1.292 ± 0.86, respectively). In addition we observed significantly more migration in 5% O_2 compared to 20% O_2 (0.404 ± 0.184 compared to 0.008 ± 0.004, respectively) (Fig. 4. 3A and B).

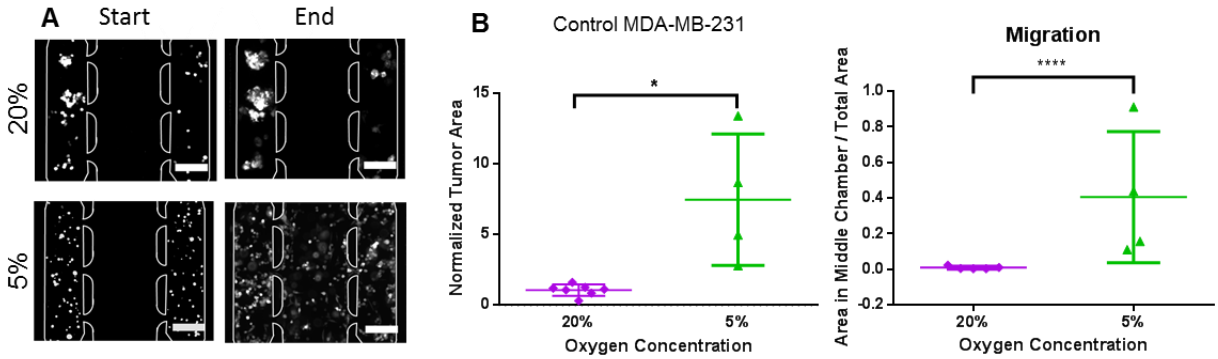

Fig. 4. 3 There is enhanced tumor progression at 5% O_2 compared to 20% 0_2 for Control MDA-MB-231 cells. (A) Images of representative devices in 20% (purple) vs. 5% O_2 (green). (B) Quantification of normalized tumor area (left) and migration (right). *, $p < 0.05$; ****, $p < 0.0001$. Scale bar: 200 μm.

Furthermore, when applying the oxygen gradient to the Control cells, there was no significant difference between the side that experienced the oxygen gradient (left) and the normoxia side (right). After flowing a 1mM sodium sulfite near the left tissue chamber, the left tissue chamber had a NTA of 6.4 ± 2.8 compared to the right chamber of 4.4 ± 1.9. Increasing the oxygen scavenger concentration to 2mM, the left and right chambers had a NTA of 5.8 ± 2.6 and 6.5 ± 1.4 respectively. The 3 mM case had a NTA of 4.8 ± 2.6 in the left and 3.7 ± 1.2 in the right chamber. Lastly, increasing the sodium sulfite concentration to 5mM had a NTA of 4.6 ± 3.0 and 6.3 ± 3.3 in the left and right chambers respectively. In all these conditions, there was no statistical significance between the left and right sides (Fig. 4. 4A).

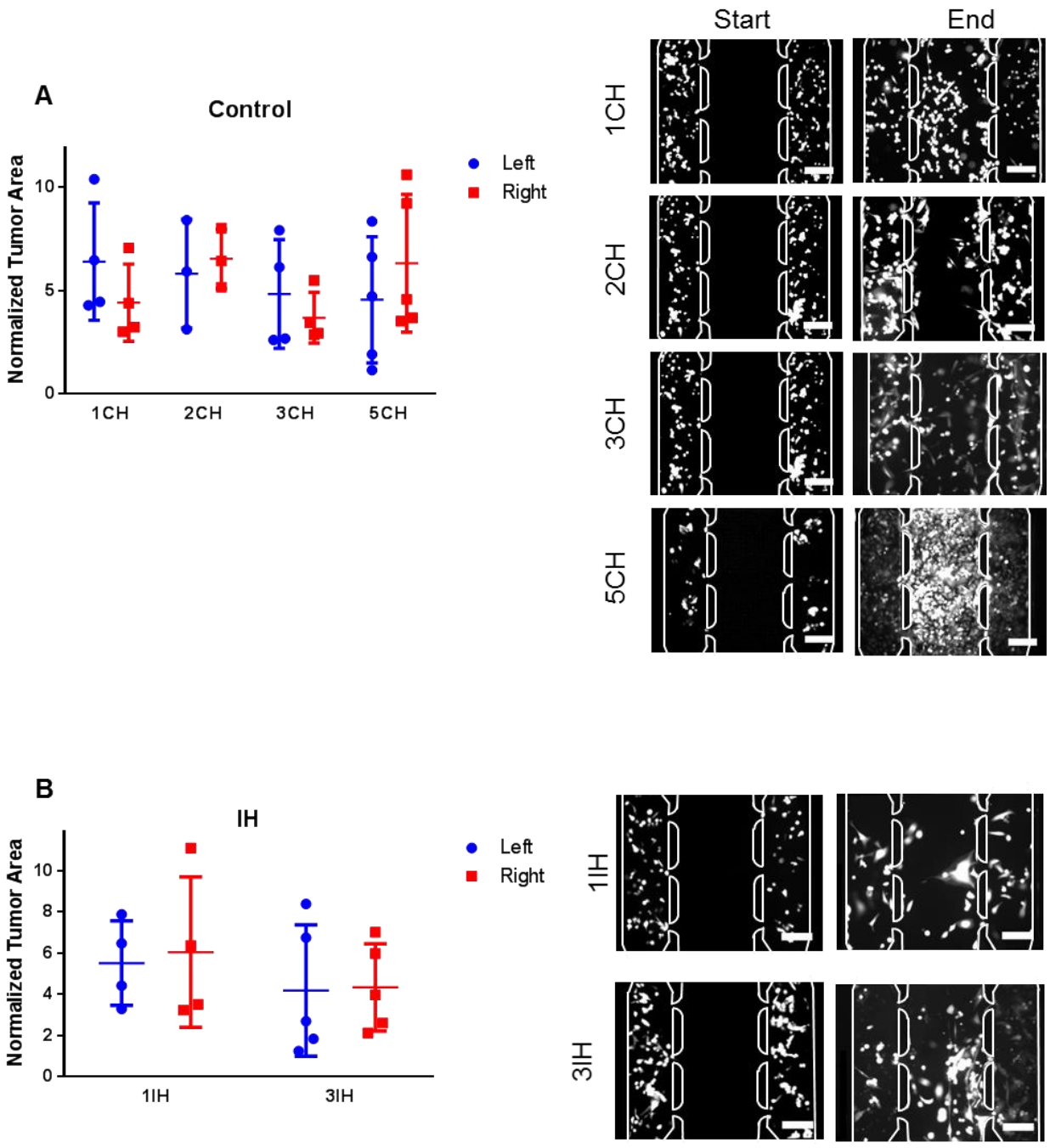

Fig. 4. 4 Varying spatial and temporal gradients do not affect Control cell survival. (A) Chronic hypoxia conditions were defined by flowing varying concentrations of sodium sulfite from 1mM (1CH), 2mM (2CH), 3mM (3CH), and 5mM (5CH). Normalized tumor area (NTA) was compared from the left chamber (blue, hypoxic side) to the right chamber (red, normoxic side). There was no statistical significance between the two sides (left graph). Images from each condition is shown on the right. The image in the left column is before the treatment of oxygen scavenger and the image in the right column is after the treatment. (B) Intermittent hypoxia conditions were defined to have the same temporal oxygen concentration gradient of flowing 1mM or 3mM of scavenger constantly (termed 1IH and

3IH respectively). Quantification of NTA (left graph) showed no statistical significance between the left (hypoxic) and right (normoxic side). Representative images of the experimental conditions are shown with images on the right. Scale bar: 200 μm.

In addition, there was also no significant difference between the NTA of Control cells in the two sides of the device under the intermittent hypoxia conditions. The 1IH condition had a NTA of 5.5 ± 2.0 and 6.0 ± 3.6 in the left and right chambers respectively. In the 3IH conditions, there was also no statistical significance in NTA between the left (4.2 ± 3.1) and right (4.3 ± 2.1) chambers (Fig. 4. 4B).

4.4.3 Scramble and shHIF-1α Growth under Varying Oxygen Gradients

After transducing the MDA-MB-231 cells with shRNA for HIF-1α, we observed an approximate 60% knockdown of gene expression of HIF-1α in the shHIF-1α cells compared to Control (Fig. 4. 5). Knockdown of HIF-1α abrogated tumor cell growth at 5% oxygen such that there was no longer any difference in growth compared to 20%. (NTA 1.8 ± 0.6 compared to 1.1 ± 0.3 for 20% and 5% O_2, respectively) (Fig. 4. 6A and B). Similarly, there was no difference in migration between 20% and 5% O_2 (0.25 ± 0.16 and 0.09 ±0.11 respectively).

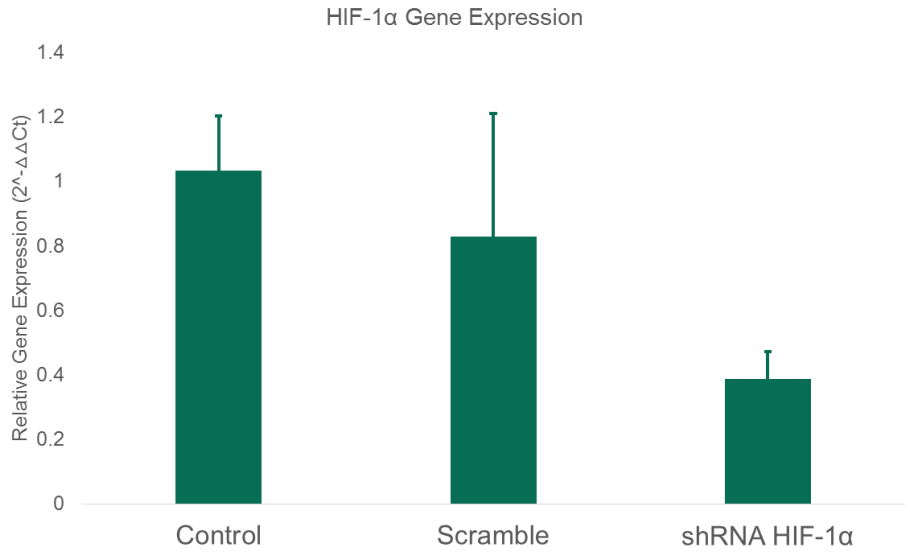

Fig. 4. 5 Relative Gene Expression of Scramble and shRNA HIF-1α cells. Data from the qRT-PCR showed that knockdown cells had roughly a 60% reduced expression of HIF-1α.

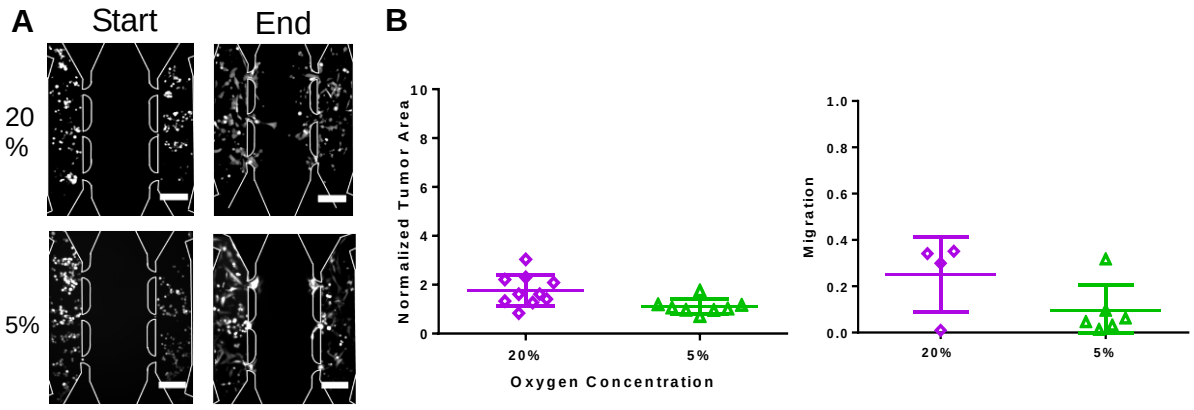

Fig. 4. 6 Knockdown of HIF-1α impacts tumor progression at normoxia (A) Images of devices in the 20% O_2 (top) and 5% O_2 (bottom) at the start (left column) and end (right column) of the experiment. (B) Quantification of NTA (left) and migration (right) shows no statistical difference between devices grown at 20% O_2 (purple) or 5% O_2 (green) with shHIF-1α cells.

Knockdown of HIF-1α significantly impacted the response to spatial and time varying oxygen concentration. First, there was no significant difference in tumor growth between the left and right side of the chambers for 0, 1mM, or 2mM sodium sulfite (Fig. 4. 7). 3mM sodium sulfite did not impact the Scramble cells (NTA of 3.7 ± 3.7 (left) and 4.0 ± 2.3 (right)); however, the tumor cells in the left side (lower oxygen) of the shHIF-1α demonstrated less growth (0.8 ± 0.2 compared to 2.3 ± 0.9 in the left and right chambers, respectively, $p < 0.05$) (Fig. 4. 7D). A similar trend was observed at 5mM sodium sulfite (4.5 ± 1.3 and 5.1 ± 0.7 respectively for the Scramble, but 0.8 ± 0.7 and 3.0 ± 2.4 for the shHIF-1α, respectively, $p < 0.01$) (Fig. 4. 7E). Additionally, Fig. 4. 8 shows the percentage of tumor growth in the left and right chambers for the shHIF-1α cells. This was calculated by dividing the tumor area in the left or right chamber by the total tumor area in the final day of the experiment. The tumor growth of the shHIF-1α cells becomes severely impacted in the 3CH and 5CH conditions.

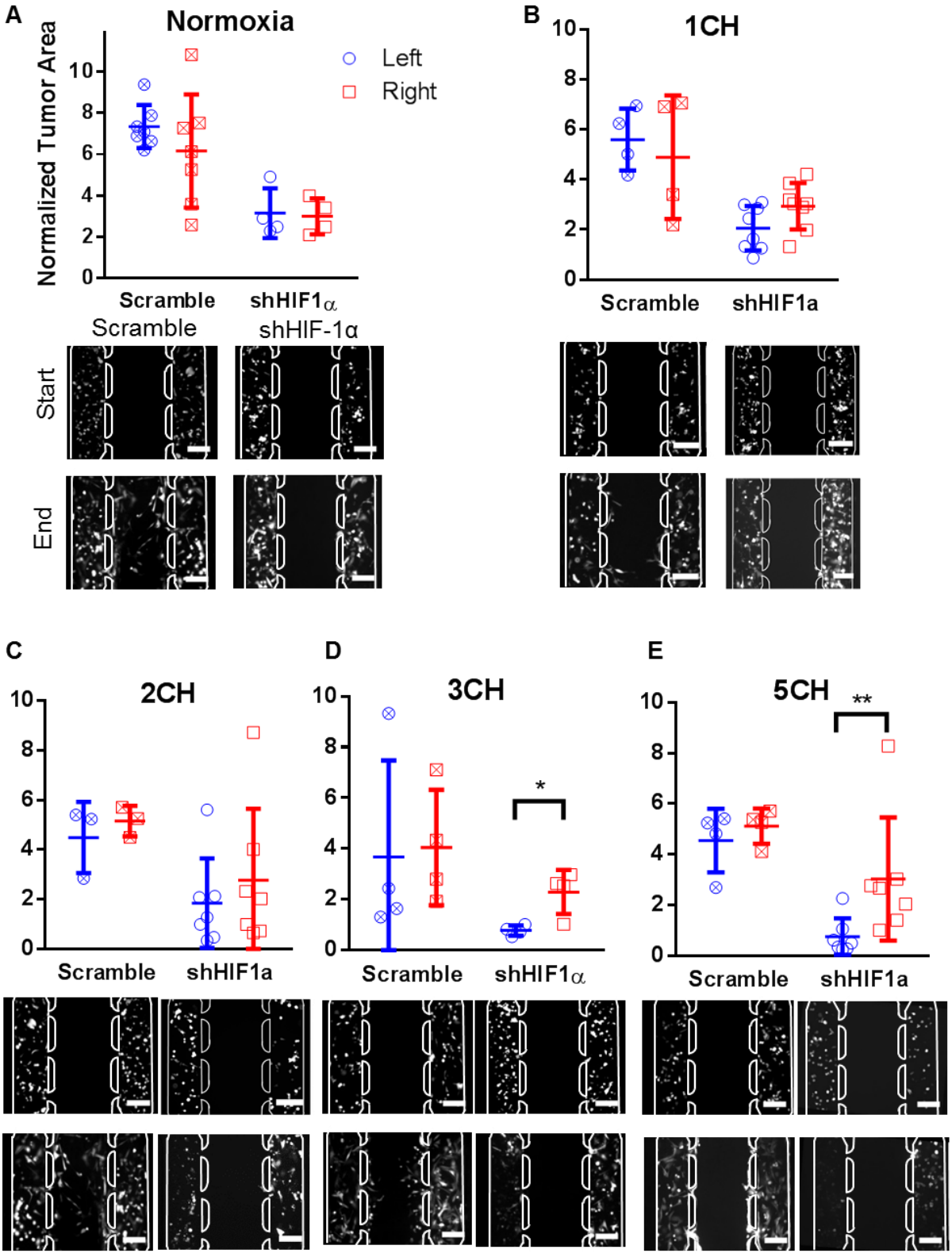

Fig. 4. 7 Various oxygen concentration gradients modulate the survival of MDA-MB-231 cells with a knockdown of HIF-1α. (A-E) Quantification of NTA for Scramble and shHIF-1α in various chronic hypoxia conditions (top graph).

Scramble (left) and shHIF-1α (right) images before (top) and after (bottom) treatment are shown below. (A) Normoxia had no statistical difference between the left and right chambers for both the Scramble and shHIF-1α cells. (B) 1CH and (C) 2CH also had no statistical difference between the left and right chambers. (D) At 3CH, Scramble had no statistical difference between the two chambers, but shHIF-1α had statistically less growth in the left (hypoxic) chamber compared to the right. (E) 5CH had no statistical difference between the left and right chambers for the Scramble cells, but had statistically significant difference between the two for the shHIF-1α cells. Left chambers are represented in blue and right chambers are represented in red for Scramble (cross) and shHIF-1α (blank) cells. *, $p < 0.05$; **, $p < .01$. Scale bar = 200 μm.

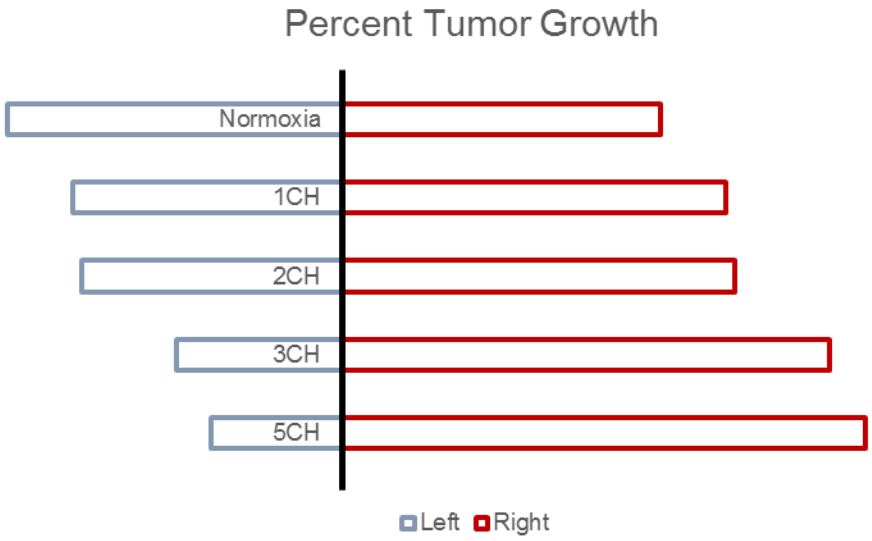

Fig. 4. 8 Percent tumor growth of shHIF-1α. As the concentration of sodium sulfite increases, the more it impacts the tumor cell growth in the left chamber. At 3CH and 5CH conditions, this impact becomes significant.

The cycles of intermittent hypoxia were performed to produce an oxygen tension with a temporal average similar to the 1mM or 3mM CH condition. These conditions are termed 1IH and 3IH, respectively. For our conditions, we used a ratio of 1:1 for the duration of applying the scavenger to stopping the flow of scavenger. For 1IH, we applied long 12 hour cycles and saw no significant difference between the two sides of the Scramble case (NTA of 3.4 ± 2.5 and 4.1 ± 1.2, respectively, for the left and right side of the device). However, with this longer 12 hour cycle duration, we saw a significant difference between the left and right sides of the device in the shHIF-1α case (NTA of 0.4 ± 0.2 and 2.1 ± 0.9, respectively, $p < 0.05$) (Fig. 4. 9A). With the 3IH condition, we used shorter 1 hour cycles of alternating scavenger flow and no flow. In this

case, we saw no significant difference in either the Scramble (NTA of 4.3 ± 0.9 and 4.3 ± 1.0 for the left and right sides, respectively) or the shHIF-1α condition (NTA of 3.0 ± 2.6 (left) and 3.7 ± 2.5 (right)) (Fig. 4. 9B).

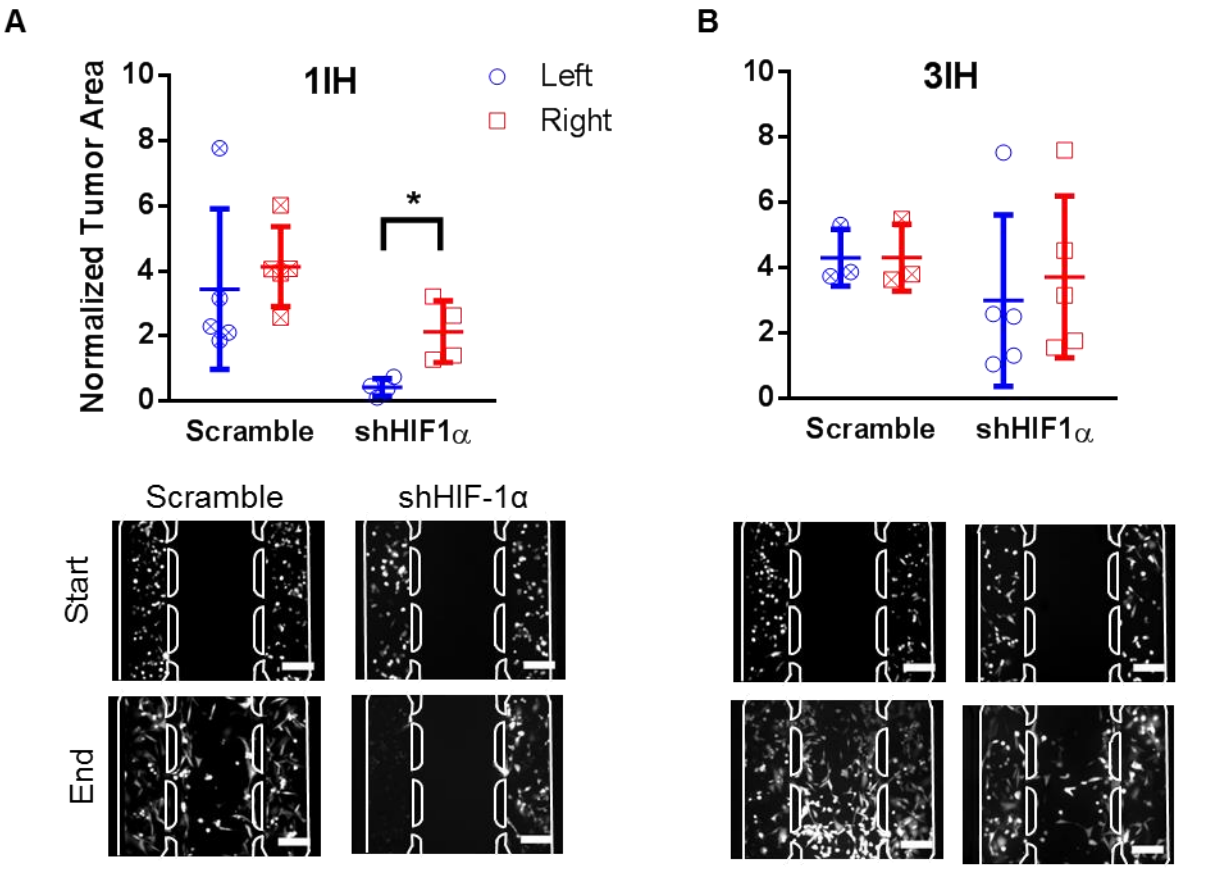

Fig. 4. 9 Temporal variations in oxygen tension affect the survival of shHIF-1α cells. (A-B) NTA is shown in the upper graph, while representative images are shown below. (A) In the 1IH case, there was no statistical significance between the growth in the left or right chambers of the Scramble cells. There was statistical significance in growth between the left and right chambers for the shHIF-1α cells. (B) The 3IH condition had no statistical difference between the left and right chambers in the Scramble and shHIF-1α cells. Left chambers are represented in blue and right chambers are represented in red for Scramble (cross) and shHIF-1α (blank) cells. *, $p < 0.05$. Scale bar = 200 μm.

4.4.4 Migration parameter during hypoxic conditions

In addition to tumor growth, we measured tumor migration into the central chamber (Fig. 4. 10). The Control cells had relatively similar migration values over all the conditions (averaging 0.42 ± 0.18). In contrast, shHIF-1α cells had more variable migration values. Starting with normoxia, the shHIF-1α cells had a migration parameter of 0.14 ± 0.09. The 5CH condition had no

migration and the 3IH condition had the most migration with a value of 0.136 ± 0.19. Overall, the Control cells had significantly more migration than the shHIF-1α cells except for the 4IH condition, which had a p-value of 0.06. Lastly, the Scramble cells had similar migration values to the Control cells with an average value of 0.3 ± 0.19 over all the conditions. There was no significant difference between the Control and Scramble migration values.

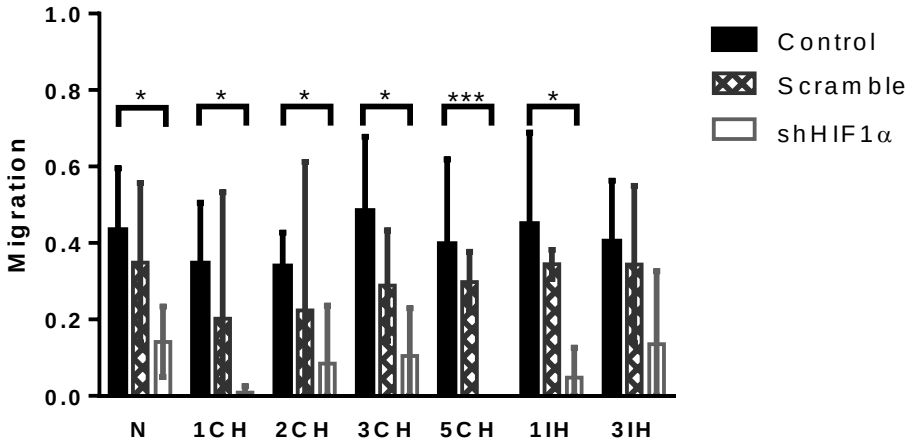

Fig. 4. 10 Knockdown of HIF-1α impacts the migration of MDA-MB-231 cells. Quantification of migration for each oxygen gradient condition for the Control (black), Scramble (crisscross), and shHIF-1α (white) cells. In all conditions except for 3IH, the Control cells had statistically significant more migration than shHIF-1α (*, $p < 0.05$ and ***, $p < .001$).

4.5 Discussion

As organ-on-a-chip technologies have become more advanced, there is a growing interest to replicate disease states.[77] However, disease states can be difficult to recapitulate due to their complexity relative to normal physiology. During tumor progression, the rapid growth of tumor cells requires an expanding vessel network to provide nutrients and oxygen to the growing mass.[10] However, the resulting vessel network is often leaky and tortuous.[78] This difference in vasculature network can lead to abnormal temporal and spatial oxygen gradients, and those tumor cells that can persist in hypoxic microenvironments have been shown to be resistant to traditional cancer treatments. Our study presents the design, fabrication, and testing of a

microfluidic device that can control oxygen gradients both spatially and temporally. We have shown that this device can be used to investigate mechanisms of hypoxia, such as the role of HIF-1α in modulating temporal dynamics of oxygen concentration.

Our initial observation that MDA-MB-231 breast cancer cells have more growth and migration in 5% O_2 than 20% O_2 suggests that these cells have adapted to have a survival advantage at a normoxic oxygen tension. Knocking down HIF-1α completely abrogates this growth advantage suggesting that MDA-MB-231 cells have a higher level of HIF-1α at normoxic oxygen levels.

To begin to understand the mechanisms that contribute to an enhanced level of HIF-1α, we applied varying spatial and temporal oxygen gradients to Control, Scramble and shHIF-1α cells. Our results for chronic hypoxia (not temporal variation) show that an observable change in tumor cell growth can be detected within a very small range of oxygen tensions. There was no detectable change in growth at 2 mM sodium sulfite (mean oxygen tension in the scavenger side tumor chamber of 4.93%), yet 3mM sodium sulfite (mean oxygen tension in the scavenger side tumor chamber of 4.90%) produced a significant reduction in growth. In other words, HIF-1α provides a threshold oxygen concentration for enhanced MDA-MB-231 cancer cell growth.

Using equal cycles of scavenger flow and no flow, we chose intermittent hypoxic conditions that have the same temporal average of 1CH and 3CH conditions. We chose these conditions because they were near the threshold of showing no bias (1CH) or significant bias (3CH) between the left and right shHIF-1α tissue chambers. Interestingly, although 1CH showed no variance between the two sides, 1IH showed a significant difference between the left and right chambers. Under this condition, a long cycle (12 hours) of 3mM scavenger flow followed by no flow was adequate to induce a similar response of a constant 3mM sodium sulfite. In contrast, even though 3CH had significant variation in tumor growth between the left and right chambers in the

shHIF-1α condition, by choosing a relatively short cycle of 1 hour of scavenger flow and no flow, the 3IH condition showed no significant difference. This is interesting because although the temporal average oxygen concentration is the same between the corresponding chronic and intermittent hypoxia conditions, the outcomes from the shHIF-1α differ in these two cases. This result provides some insight into the necessary duration of hypoxia at the level of 4.9% to impact cell proliferation: the duration should be longer than 1 hour, and 12 hours is adequate.

Lastly, we quantified a migration parameter between the Control, Scramble, and shHIF-1α. We found that there was statistically more tumor migration in the Control cells than shHIF-1α in every condition except for 3IH, which had p-value of 0.06. This is consistent with previous studies that show that HIF-1α stimulates tumor migration.[79,80] While we didn't see any trends in tumor migration between the different hypoxic conditions, it would be of interest to use different fluorescent MDA-MB-231 cells in the left and right chambers to identify if more cells were migrating from the left (hypoxic) chamber or the right (normoxia) chamber.

4.6 Conclusions

The aim of this study was to demonstrate the need to more accurately recapitulate the tumor microenvironment for effective drug testing. We chose to control oxygen tension both temporally and spatially and then examined tumor cell proliferation and migration -- indices of tumor progression. While an attractive target of tumor hypoxia is HIF-1α, we have demonstrated that the spatial and temporal complexities of the oxygen environment can potentially undermine this strategy. Because the microfluidic device design we used has the ability to measure tumor growth and migration throughout the length of the experiment, we were able to quantify tumor progression over the course of oxygen treatment. Overall, we believe this microfluidic design is

flexible enough to recapitulate some of the intricacies of the tumor microenvironment to give us the opportunity to study tumor behavior under varying oxygen tensions.

Chapter 5: Conclusions and Future Directions

Since the first discovery of the cause of a cancer in 1731, many advancements have been made to understand this disease.[81] However, with each new discovery, we uncover so much more that we do not understand. This creates many problems while trying to discover and test new cancer treatments. Therefore, it is critical for scientists to develop platforms that can best recreate the tumor microenvironment for both research and drug innovation applications.

5.1 Tumor-on-a-chip Systems

Microengineered physiological systems have become a promising technology for drug testing as well as studying tumor biology.[82] Due to its inherent small size, this approach reduces reagent requirements which facilitates high-throughput testing, which is critical for anticancer drug pre-screening applications. In addition, because most microphysiological systems are developed using a clear plastic, researchers have the opportunity to watch tumor progression in terms of growth, invasion, and metastasis in real time.[83] This provides a huge advantage over animal models, which is the current gold standard. While animal models can sustain complex tumor microenvironments, it is unclear how accurately it can model human tumorigenesis.[84] Thus, there is great interest in developing better tumor models.

The tumor microenvironment consists of a complex mixture of cellular and non-cellular components. The surrounding environment can include blood vessels, carcinoma associated fibroblasts (CAFs), immune cells, and the extracellular matrix. It has become increasingly recognized that the key to developing cancer treatments is our ability to recapitulate these aspects of the tumor microenvironment. Recent studies have shown that the interaction between tumor

cells and microenvironment has profound effects on the tumor's behavior and drug resistance.[85,86] Many advancements have been made towards including the heterogeneous mixture of cell types in the tumor microenvironment. Qin's research lab used the high spatial control of microfluidic devices to study how CAFs promote tumor spheroid invasion.[87] Jeon's research group has developed a method for studying the process of tumor angiogenesis and how tumor cells interact with the blood vessel network, which has implications for understanding tumor metastasis.[88] Furthermore, Businaro's research group has studied the interaction between tumor cells and the immune system to observe that the tumor cells can direct the migration of the immune cells.[89] Together, these groups have demonstrated that microphysiological systems can incorporate multiple cell types to study their interaction during tumor progression.

Another important aspect to replicate in the tumor microenvironment is the tumor cells interaction with non-cellular components. Often, this consists of mimicking the extracellular matrix that's present in the tumor microenvironment. It has been known that the matrix stiffness increases in the tumor microenvironment. These parameters are easily modulated in microengineered physiological systems, and Weaver's research group has shown that by replicating the increased stiffness of the extracellular matrix of the tumor microenvironment, it promotes a more malignant behavior by modulating integrins, which is critical for our understanding of cancer cell migration.[90] Other studies have looked at how chemical gradients affect tumor behavior.[59,91] However, an important aspect of tumor biology to replicate is tumor hypoxia, which has been proven to be difficult to model.

5.2 Hypoxia Disease Modelling

Several strategies have been used to mimic hypoxia for disease modelling. One strategy from Gerecht's lab has been to develop a hydrogel that consumes oxygen *in situ*.[92] They have shown that their hypoxic hydrogels can promote neovascularization from a host tissue during subcutaneous wound healing.[92] McGuigan's lab discovered a method of turning two-dimensional cell cultures in to three-dimensional models of tumors by rolling a scaffold-tumor strip into a cylinder. A gradient of oxygen then forms from the outside of the cylinder towards the center as it is diffusion limited. By unrolling the strip, the research team showed that they were able to understand the spatial mapping of cell metabolism within a tumor sphere.[93] Another method of modelling tumor hypoxia comes from the Whitesides' lab and was termed Cells-in-Gels-in-Paper (CiGiP). This method employs the layering of stacks of paper containing cells encapsulated in a gel with the lower layers receiving less oxygen and nutrients than the top layers. The research team identified that after deconstruction of the different layers, the bottom (hypoxic) cells were more resistant to irradiation treatment.[94]

A trend for studying hypoxia has been to use microfluidic devices. With inherently small features, there are very short diffusion times to manipulate oxygen tension. As mentioned in Chapter 2, there are several strategies that employ microfluidic devices to control oxygen gradients. Most include using a dedicated line for an oxygen sink to draw oxygen away from the tissue chamber. This can be nitrogen gas, a chemical reaction, or another cell type consuming oxygen. Chapters 3 and 4 detail a method of using sodium sulfite as a scavenger to control the spatial and temporal gradients of oxygen. For all of these designs, an important consideration for choosing an oxygen scavenger is the reaction rate. Because we wanted to switch the flow of scavenger on and off quickly, we chose a scavenger that can react with oxygen quickly.

5.3 Future Directions

Over the past 5 years, there has been increasing interest in using microphysiological systems to resolve some of the critical issues in drug development. The more we can advance these models of the human body, the more applicable they become to studying human physiology and pathology. In the future, as more accurate models of tumor hypoxia become available, we can begin to study how tumor metabolism adapts to these pressures. The ability for cancer cells to alter their metabolism is one of the reasons tumors can thrive during hypoxia, and these changes are now considered one of the hallmark features of cancer.[95] This understanding of tumor metabolism during hypoxia can give researchers new therapeutic targets. Furthermore, by creating an accurate microfluidic device of tumor hypoxia, we can use this platform as a high throughput method of testing the effectiveness of drugs to target hypoxia cancer cells. As these are understood to be the hardest cells to target, developing an accurate model for tumor hypoxia can help resolve these issues. While many challenges remain for developing chronic and intermittent hypoxia, there remains growing interest to address these challenges and present new and exciting opportunities for improved anticancer therapies.

References

1. Siegel, R. L., Miller, K. D. & Jemal, A. Cancer statistics, 2018. *CA. Cancer J. Clin.* **68,** 7–30 (2018).

2. Heron, M. & Anderson, R. N. Changes in the Leading Cause of Death: Recent Patterns in Heart Disease and Cancer Mortality. *NCHS Data Brief* **254,** 1–8 (2016).

3. Carter, A. J. & Nguyen, C. N. A comparison of cancer burden and research spending reveals discrepancies in the distribution of research funding. *BMC Public Health* **12,** (2012).

4. DiMasi, J. A., Grabowski, H. G. & Hansen, R. W. Innovation in the pharmaceutical industry: New estimates of R&D costs. *J. Health Econ.* **47,** 20–33 (2016).

5. Sertkaya, A., Wong, H.-H., Jessup, A. & Beleche, T. Key cost drivers of pharmaceutical clinical trials in the United States. *Clin. Trials* **13,** 117–126 (2016).

6. Folkman, J. Tumor angiogenesis: therapeutic implications. *N. Engl. J. Med.* **285,** 1182–6 (1971).

7. Hanahan, D. & Weinberg, R. A. Review Hallmarks of Cancer : The Next Generation. *Cell* **144,** 646–674 (2011).

8. Breast Cancer Survival Rates. at <https://www.cancer.org/cancer/breast-cancer/understanding-a-breast-cancer-diagnosis/breast-cancer-survival-rates.html>

9. Yang, Y., Sun, M., Wang, L. & Jiao, B. HIFs, angiogenesis, and cancer. *J. Cell. Biochem.* **114,** 967–74 (2013).

10. Vaupel, P., Mayer, A. & Höckel, M. Tumor hypoxia and malignant progression. *Methods Enzymol.* **381,** 335–54 (2004).

11. Wang, G. L., Jiang, B. H., Rue, E. A. & Semenza, G. L. Hypoxia-inducible factor 1 is a basic-helix-loop-helix-PAS heterodimer regulated by cellular O2 tension. *Proc. Natl. Acad. Sci.* **92,** 5510–5514 (1995).

12. Byrne, M. B., Leslie, M. T., Gaskins, H. R. & Kenis, P. J. A. Methods to study the tumor microenvironment under controlled oxygen conditions. *Trends Biotechnol.* **32,** 556–563 (2014).

13. Xie, J. *et al.* Hypoxia regulates stemness of breast cancer MDA-MB-231 cells. *Med. Oncol.* **33,** 1–7 (2016).

14. Wu, D. & Yotnda, P. Induction and testing of hypoxia in cell culture. *J. Vis. Exp.* (2011). doi:10.3791/2899

15. PIRET, J.-P., MOTTET, D., RAES, M. & MICHIELS, C. CoCl 2 , a Chemical Inducer of Hypoxia-Inducible Factor-1, and Hypoxia Reduce Apoptotic Cell Death in Hepatoma Cell Line HepG2. *Ann. N. Y. Acad. Sci.* **973,** 443–447 (2002).

16. Dewhirst, M. W., Braun, R. D. & Lanzen, J. L. Temporal changes in pO2 of R3230Ac tumors in fischer-344 rats. *Int. J. Radiat. Oncol.* **42,** 723–726 (1998).

17. Gilkes, D. M., Semenza, G. L. & Wirtz, D. Hypoxia and the extracellular matrix: drivers of tumour metastasis. *Nat Rev Cancer* **14,** 430–439 (2014).

18. Harris, A. L. Hypoxia — a key regulatory factor in tumour growth. *Nat Rev Cancer* **2,** 38–47 (2002).

19. Baudino, T. A. *et al.* c-Myc is essential for vasculogenesis and angiogenesis during development and tumor progression. *Genes Dev.* **16,** 2530–43 (2002).

20. Grimes, D. R., Kelly, C., Bloch, K. & Partridge, M. A method for estimating the oxygen consumption rate in multicellular tumour spheroids. *J. R. Soc. Interface* **11,** 20131124 (2014).

21. Liao, D. & Johnson, R. S. Hypoxia: a key regulator of angiogenesis in cancer. *Cancer Metastasis Rev.* **26,** 281–90 (2007).

22. Semenza, G. L. Hypoxia-inducible factors: mediators of cancer progression and targets for cancer therapy. *Trends Pharmacol. Sci.* **33,** 207–14 (2012).

23. Carmeliet, P. Angiogenesis in health and disease. *Nat. Med.* **9,** 653–60 (2003).

24. Zhou, W. *et al.* Assessment of hypoxia inducible factor levels in cancer cell lines upon hypoxic induction using a novel reporter construct. *PLoS One* **6,** e27460 (2011).

25. Krock, B. L., Skuli, N. & Simon, M. C. Hypoxia-Induced Angiogenesis: Good and Evil. *Genes Cancer* **2,** 1117–1133 (2011).

26. Funamoto, K. *et al.* A novel microfluidic platform for high-resolution imaging of a three-dimensional cell culture under a controlled hypoxic environment. *Lab Chip* **12,** 4855 (2012).

27. Brennan, M. D., Rexius-Hall, M. L., Elgass, L. J. & Eddington, D. T. Oxygen control with microfluidics. *Lab Chip* **14,** 4305–4318 (2014).

28. Wang, L. *et al.* Construction of oxygen and chemical concentration gradients in a single microfluidic device for studying tumor cell–drug interactions in a dynamic hypoxia microenvironment. *Lab Chip* **13,** 695–705 (2013).

29. Ochs, C. J., Kasuya, J., Pavesi, A. & Kamm, R. D. Oxygen levels in thermoplastic microfluidic devices during cell culture. *Lab Chip* **14,** 459–462 (2013).

30. Clark, L. C. & Lyons, C. ELECTRODE SYSTEMS FOR CONTINUOUS MONITORING IN CARDIOVASCULAR SURGERY. *Ann. N. Y. Acad. Sci.* **102,** 29–45

(2006).

31. Esipova, T. V *et al.* Two new ‘protected’ oxyphors for biological oximetry: properties and application in tumor imaging. *Anal. Chem.* **83,** 8756–65 (2011).

32. Griffith, C. K. *et al.* Diffusion Limits of an in Vitro Thick Prevascularized Tissue. *Tissue Eng.* **11,** 257–266 (2005).

33. Carmeliet, P. & Jain, R. K. Angiogenesis in cancer and other diseases. *Nature* **407,** 249 (2000).

34. Goodall, C. M., Sanders, A. G. & Shubik, P. Studies of Vascular Patterns in Living Tumors With a Transparent Chamber Inserted in Hamster Cheek Pouch2. *JNCI J. Natl. Cancer Inst.* **35,** 497–521 (1965).

35. Semenza, G. L. Oxygen Sensing, Hypoxia-Inducible Factors, and Disease Pathophysiology. *Annu. Rev. Pathol. Mech. Dis.* **9,** 47–71 (2014).

36. Rofstad, E. K., Galappathi, K., Mathiesen, B. & Ruud, E. B. M. Fluctuating and diffusion-limited hypoxia in hypoxia-induced metastasis. *Clin. Cancer Res.* **13,** 1971–1978 (2007).

37. Stavri, G. T., Zachary, I. C., Baskerville, P. A., Martin, J. F. & Erusalimsky, J. D. Basic Fibroblast Growth Factor Upregulates the Expression of Vascular Endothelial Growth Factor in Vascular Smooth Muscle Cells : Synergistic Interaction With Hypoxia. *Circulation* **92,** 11–14 (1995).

38. Gurdon, J. B. & Bourillot, P.-Y. Morphogen gradient interpretation. *Nature* **413,** 797–803 (2001).

39. Helm, C.-L. E., Fleury, M. E., Zisch, A. H., Boschetti, F. & Swartz, M. A. Synergy between interstitial flow and VEGF directs capillary morphogenesis in vitro through a gradient amplification mechanism. *Proc. Natl. Acad. Sci.* **102,** 15779–15784 (2005).

40. Lo, J. F., Sinkala, E. & Eddington, D. T. Oxygen gradients for open well cellular cultures via microfluidic substrates. *Lab Chip* **10,** 2394 (2010).

41. Germain, T., Ansari, M. & Pappas, D. Observation of reversible, rapid changes in drug susceptibility of hypoxic tumor cells in a microfluidic device. *Anal. Chim. Acta* **936,** 179–184 (2016).

42. Toffoli, S. *et al.* NDRG1 and CRK-I/II are regulators of endothelial cell migration under intermittent hypoxia. *Angiogenesis* **12,** 339–354 (2009).

43. Tellier, C. *et al.* Cycling Hypoxia Induces a Specific Amplified Inflammatory Phenotype in Endothelial Cells and Enhances Tumor-Promoting Inflammation In Vivo. *Neoplasia* **17,** 66–78 (2015).

44. Lo, J. F. *et al.* Islet Preconditioning via Multimodal Microfluidic Modulation of Intermittent Hypoxia. *Anal. Chem.* **84,** 1987–1993 (2012).

45. Chen, Y.-A. *et al.* Generation of oxygen gradients in microfluidic devices for cell culture using spatially confined chemical reactions. *Lab Chip* **11,** 3626–33 (2011).

46. Vaupel, P., Briest, S. & Hockel, M. Hypoxia in Breast Cancer: Pathogenesis, Characterization and Biological/Therapeutic Implications. *Wiener Medizinische Wochenschrift* **152,** 334–342 (2002).

47. Ehsan, S. M. & George, S. C. Nonsteady State Oxygen Transport in Engineered Tissue: Implications for Design. *Tissue Eng. Part A* **19,** 1433–1442 (2013).

48. Buchwald, P. FEM-based oxygen consumption and cell viability models for avascular pancreatic islets. *Theor. Biol. Med. Model.* **6,** 5 (2009).

49. Hsu, Y.-H. *et al.* Full range physiological mass transport control in 3D tissue cultures. *Lab Chip* **13,** 81–89 (2013).

50. Moya, M. L., Hsu, Y.-H., Lee, A. P., Hughes, C. C. W. & George, S. C. In Vitro Perfused Human Capillary Networks. *Tissue Eng. Part C Methods* **19,** 730–737 (2013).

51. Hsu, Y.-H., Moya, M. L., Hughes, C. C. W., George, S. C. & Lee, A. P. A microfluidic platform for generating large-scale nearly identical human microphysiological vascularized tissue arrays. *Lab Chip* **13,** 2990 (2013).

52. Barron, C. H. & O'Hern, H. a. Reaction kinetics of sodium sulfite oxidation by the rapid-mixing method. *Chem. Eng. Sci.* **21,** 397–404 (1966).

53. Hui, P. K. & Palmer, H. J. Uncatalyzed oxidation of aqueous sodium sulfite and its ability to simulate bacterial respiration. *Biotechnol. Bioeng.* **37,** 392–396 (1991).

54. Cox, M. E. & Dunn, B. Oxygen diffusion in poly(dimethyl siloxane) using fluorescence quenching. I. Measurement technique and analysis. *J. Polym. Sci. Part A Polym. Chem.* **24,** 621–636 (1986).

55. Digman, M. a, Caiolfa, V. R., Zamai, M. & Gratton, E. The phasor approach to fluorescence lifetime imaging analysis. *Biophys. J.* **94,** L14-6 (2008).

56. White, S. M. *et al.* Implanted Cell-Dense Prevascularized Tissues Develop Functional Vasculature That Supports Reoxygenation After Thrombosis. *Tissue Eng. Part A* **20,** 2316–2328 (2014).

57. Moya, M., Tran, D. & George, S. C. An integrated in vitro model of perfused tumor and cardiac tissue. *Stem Cell Res. Ther.* **4 Suppl 1,** S15 (2013).

58. Moya, M. L., Alonzo, L. F. & George, S. C. Microfluidic device to culture 3D in vitro human capillary networks. *Methods Mol. Biol.* **1202,** 21–7 (2014).

59. Shirure, V. S., Lezia, A., Tao, A., Alonzo, L. F. & George, S. C. Low levels of physiological interstitial flow eliminate morphogen gradients and guide angiogenesis. *Angiogenesis* **20,** 493–504 (2017).

60. Alonzo, L. F., Moya, M. L., Shirure, V. S. & George, S. C. Microfluidic device to control interstitial flow-mediated homotypic and heterotypic cellular communication. *Lab Chip* (2015). doi:10.1039/c5lc00507h

61. Gaustad, J. V., Simonsen, T. G., Roa, A. M. A. & Rofstad, E. K. Tumors exposed to acute cyclic hypoxia show increased vessel density and delayed blood supply. *Microvasc. Res.* **85,** 10–15 (2013).

62. Carmeliet, P. & Jain, R. K. Angiogenesis in cancer and other diseases. *Nature* **407,** 249–257 (2000).

63. Ehsan, S. M. & George, S. C. Vessel network formation in response to intermittent hypoxia is frequency dependent. *J. Biosci. Bioeng.* **120,** 347–350 (2015).

64. Vaupel, P. Tumor Hypoxia: Causative Factors, Compensatory Mechanisms, and Cellular Response. *Oncologist* **9,** 4–9 (2004).

65. Vaupel, P. & Mayer, A. Hypoxia in cancer: significance and impact on clinical outcome. *Cancer Metastasis Rev* **26,** 225–239 (2007).

66. Majmundar, A. J., Wong, W. J. & Simon, M. C. Hypoxia-Inducible Factors and the Response to Hypoxic Stress. *Mol. Cell* **40,** 294–309 (2010).

67. Peng, Y.-J. *et al.* Heterozygous HIF-1α deficiency impairs carotid body-mediated systemic responses and reactive oxygen species generation in mice exposed to intermittent hypoxia. *J. Physiol.* **577,** 705–716 (2006).

68. Rofstad, E. K., Gaustad, J.-V., Egeland, T. A. M., Mathiesen, B. & Galappathi, K. Tumors exposed to acute cyclic hypoxic stress show enhanced angiogenesis, perfusion and metastatic dissemination. *Int. J. Cancer* **127,** 1535–1546 (2010).

69. Verduzco, D. *et al.* Intermittent Hypoxia Selects for Genotypes and Phenotypes That Increase Survival, Invasion, and Therapy Resistance. *PLoS One* **10,** e0120958 (2015).

70. Bhaskara, V. K., Mohanam, I., Rao, J. S. & Mohanam, S. Intermittent hypoxia regulates stem-like characteristics and differentiation of neuroblastoma cells. *PLoS One* **7,** 1–10 (2012).

71. Burroughs, S. K. *et al.* Hypoxia inducible factor pathway inhibitors as anticancer therapeutics. *Future Med. Chem.* **5,** 553–572 (2013).

72. Harrison, M. R. *et al.* Phase II study of 2-methoxyestradiol (2ME2) NanoCrystal Dispersion (NCD) in patients with taxane-refractory, metastatic hormone-refractory prostate cancer (HRPC). *J. Clin. Oncol.* **26,** 5173–5173 (2008).

73. Aeterna Zentaris Regains North American Rights to Akt Inhibitor from Keryx | GEN. at <https://www.genengnews.com/gen-news-highlights/aeterna-zentaris-regains-north-american-rights-to-akt-inhibitor-from-keryx/81246731/>

74. Hudson, C. C. *et al.* Regulation of hypoxia-inducible factor 1alpha expression and

function by the mammalian target of rapamycin. *Mol. Cell. Biol.* **22,** 7004–14 (2002).

75. Mabjeesh, N. J. *et al.* 2ME2 inhibits tumor growth and angiogenesis by disrupting microtubules and dysregulating HIF. *Cancer Cell* **3,** 363–375 (2003).

76. Feldser, D., Agani, F. & Iyer, N. V. Reciprocal Positive Regulation of Hypoxia-inducible Factor 1 α and Insulin-like Growth Factor 2 Growth Factor 2. *Cancer Res.* **59,** 3915–3918 (1999).

77. Sutherland, M. L., Fabre, K. M. & Tagle, D. a. The National Institutes of Health Microphysiological Systems Program focuses on a critical challenge in the drug discovery pipeline. *Stem Cell Res. Ther.* **4,** I1 (2013).

78. Matsumoto, S., Yasui, H., Mitchell, J. B. & Krishna, M. C. Imaging Cycling Tumor Hypoxia. *Cancer Res.* **70,** 10019–10023 (2010).

79. Liu, L. *et al.* Hypoxia‐inducible factor 1 mediates intermittent hypoxia‐induced migration of human breast cancer MDA‐MB‐231 cells. *Oncol. Lett.* **14,** 7715–7722 (2017).

80. Tátrai, E. *et al.* Cell type-dependent HIF1 α-mediated effects of hypoxia on proliferation, migration and metastatic potential of human tumor cells. *Oncotarget* **8,** 44498–44510 (2017).

81. Kipling, M. D., Usherwood, R. & Varley, R. A monstrous growth: an historical note on carcinoma of the scrotum. *Br. J. Ind. Med.* **27,** 382–4 (1970).

82. Low, L. A. & Tagle, D. A. Tissue chips – innovative tools for drug development and disease modeling. *Lab Chip* **17,** 3026–3036 (2017).

83. Heylman, C., Sobrino, A., Shirure, V. S., Hughes, C. C. & George, S. C. A strategy for integrating essential three-dimensional microphysiological systems of human organs for realistic anticancer drug screening. *Exp. Biol. Med.* **239,** 1240–1254 (2014).

84. Klausner, R. D. Studying cancer in the mouse. *Oncogene* **18,** 5249–5252 (1999).

85. Bhadriraju, K. & Chen, C. S. Engineering cellular microenvironments to improve cell-based drug testing. *Drug Discov. Today* **7,** 612–620 (2002).

86. Birgersdotter, A., Sandberg, R. & Ernberg, I. Gene expression perturbation in vitro—A growing case for three-dimensional (3D) culture systems. *Semin. Cancer Biol.* **15,** 405–412 (2005).

87. Liu, T., Lin, B. & Qin, J. Carcinoma-associated fibroblasts promoted tumor spheroid invasion on a microfluidic 3D co-culture device. *Lab Chip* **10,** 1671 (2010).

88. Kim, S., Lee, H., Chung, M. & Jeon, N. L. Engineering of functional, perfusable 3D microvascular networks on a chip. *Lab Chip* **13,** 1489 (2013).

89. Agliari, E. *et al.* Cancer-driven dynamics of immune cells in a microfluidic environment. *Sci. Rep.* **4,** 6639 (2015).

90. Paszek, M. J. *et al.* Tensional homeostasis and the malignant phenotype. *Cancer Cell* **8,** 241–254 (2005).

91. Wang, S., Saadi, W., Lin, F., Minh-Canh Nguyen, C. & Li Jeon, N. Differential effects of EGF gradient profiles on MDA-MB-231 breast cancer cell chemotaxis. *Exp. Cell Res.* **300,** 180–189 (2004).

92. Park, K. M. & Gerecht, S. Hypoxia-inducible hydrogels. *Nat. Commun.* **5,** 4075 (2014).

93. Rodenhizer, D. *et al.* A three-dimensional engineered tumour for spatial snapshot analysis of cell metabolism and phenotype in hypoxic gradients. *Nat. Mater.* **15,** (2015).

94. Simon, K. A. *et al.* Metabolic Response of Lung Cancer Cells to Radiation in a Paper-Based 3D Cell Culture System. *Biomaterials* (2016). doi:10.1016/j.biomaterials.2016.03.002

95. Fouad, Y. A. & Aanei, C. Revisiting the hallmarks of cancer. *Am. J. Cancer Res.* **7,** 1016–1036 (2017).